geodiversitas

2025 • 47 • 14

Modern and Holocene sedimentation patterns in the Persian Gulf

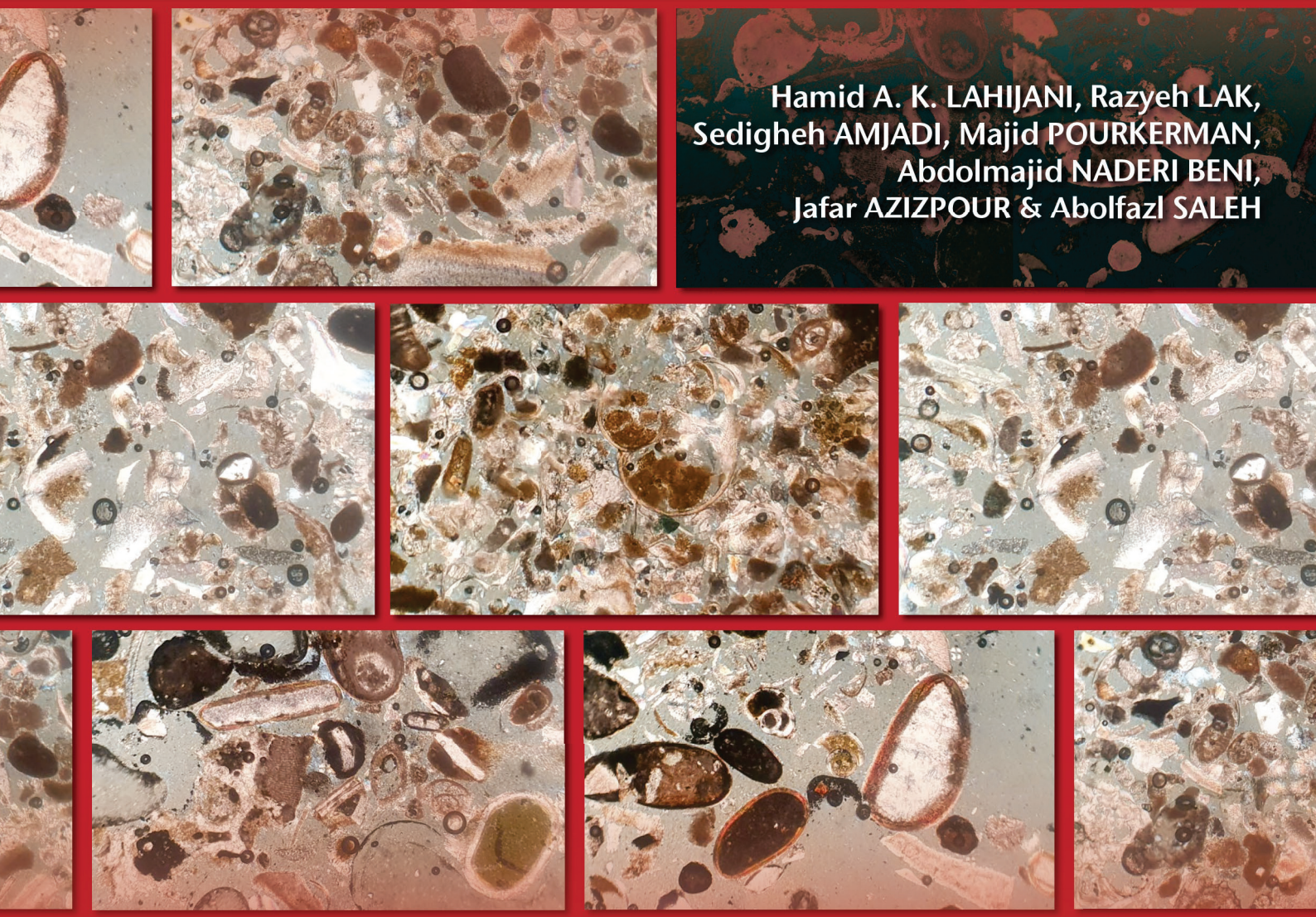

Hamid A. K. LAHIJANI, Razyeh LAK, Sedigheh AMJADI, Majid POURKERMAN, Abdolmajid NADERI BENI, Jafar AZIZPOUR & Abolfazl SALEH

art. 47 (14) — Published on 23 September 2025
www.geodiversitas.com

PUBLICATIONS SCIENTIFIQUES

MUSÉUM NAL HIST NATURELLE

Geodiversitas est indexé dans / Geodiversitas *is indexed in:*
– Science Citation Index Expanded (SciSearch®)
– ISI Alerting Services®
– Current Contents® / Physical, Chemical, and Earth Sciences®
– Scopus®

Geodiversitas est distribué en version électronique par / Geodiversitas *is distributed electronically by:*
– BioOne® (http://www.bioone.org)

Les articles ainsi que les nouveautés nomenclaturales publiés dans *Geodiversitas* sont référencés par / *Articles and nomenclatural novelties published in* Geodiversitas *are referenced by:*
– ZooBank® (http://zoobank.org)

Geodiversitas est une revue en flux continu publiée par les Publications scientifiques du Muséum, Paris
Geodiversitas *is a fast track journal published by the Museum Science Press, Paris*

Les Publications scientifiques du Muséum publient aussi / *The Museum Science Press also publish:* ***Adansonia***, ***Zoosystema***, ***Anthropozoologica***, ***European Journal of Taxonomy***, ***Naturae***, ***Cryptogamie*** **sous-sections** ***Algologie***, ***Bryologie***, ***Mycologie, Comptes Rendus Palevol***

Diffusion – Publications scientifiques Muséum national d'Histoire naturelle
CP 41 – 57 rue Cuvier F-75231 Paris cedex 05 (France)
Tél. : 33 (0)1 40 79 48 05 / Fax : 33 (0)1 40 79 38 40
diff.pub@mnhn.fr / http://sciencepress.mnhn.fr

ISSN (imprimé / *print*) : 1280-9659/ ISSN (électronique / *electronic*) : 1638-9395

Modern and Holocene sedimentation patterns in the Persian Gulf

Hamid A. K. LAHIJANI
Iranian National Institute for Oceanography and Atmospheric Science (INIOAS),
no. 3, Etemadzadeh St., Fatemi Ave, Tehran (Iran)
and Institute of Tibetan Plateau Research,
Chinese Academy of Sciences, Beijing, 100101 (China)
lahijani@inio.ac.ir (corresponding author)

Razyeh LAK
Research Institute for Earth Sciences, Geological Survey of Iran, Tehran (Iran)
lak_ir@yahoo.com (corresponding author)

Sedigheh AMJADI
Iranian National Institute for Oceanography and Atmospheric Science (INIOAS),
no. 3, Etemadzadeh St., Fatemi Ave, Tehran (Iran)

Majid POURKERMAN
Research Institute for Earth Sciences, Geological Survey of Iran, Tehran (Iran)

Abdolmajid NADERI BENI
Jafar AZIZPOUR
Abolfazl SALEH
Iranian National Institute for Oceanography and Atmospheric Science (INIOAS),
no. 3, Etemadzadeh St., Fatemi Ave, Tehran (Iran)

Submitted on 7 February 2024 | accepted on 16 September 2024 | published on 23 September 2025

urn:lsid:zoobank.org:pub:F76C75A2-3975-4847-8AEE-D61A0626BB62

Lahijani H. A. K., Lak R., Amjadi S., Pourkerman M., Naderi Beni A., Azizpour J. & Saleh A. 2025. — Modern and Holocene sedimentation patterns in the Persian Gulf. *Geodiversitas* 47 (14): 623-640. https://doi.org/10.5252/geodiversitas2025v47a14. http://geodiversias.com/47/14

ABSTRACT
The Persian Gulf (PG) being a shallow marginal sea in the northwest Indian Ocean experiences extreme environmental conditions (high seawater temperature and salinity) that impact on bottom sedimentation. To decipher the controlling parameters on sedimentation in the environment of the PG we have used a total of 25 surface sediments and three short cores, 22 coastal sediments as well as water column properties (temperature, salinity dissolved oxygen) and hydrodynamics (current velocity and direction). We applied sedimentological (grain size and type of sedimentary fractions), mineralogical (thin-section, SEM/EDS, XRD, polished-sections), and geochemical analyses (XRF core scanning). The sediments are mainly composed of silt, however sand fraction partially elevates up to around 80% and clay to 10%. Calcium carbonate and organic materials compose up to 18% and 52% of the bulk sediments, respectively. Sea floor surface sediments varies in different fractions, always with high amount of carbonates. Detrital carbonates and aluminum silicate minerals are more common in the beaches and around islands with exposed parent rocks. The core that covers the sedimentation in the Persian Gulf since the end of the Early Holocene encompasses facies representing a higher

KEY WORDS
Persian Gulf,
sedimentation,
carbonate,
hypoxia,
climate change.

biogenic carbonate signature in the base, followed by more detrital and organic matter in the middle. Sea level variations are interpreted as the primary driver of such sedimentological variations: periods of high level favored stagnant water conditions and stratification, which allowed to incorporate higher proportion of organic matter in coated grains. Both modern and Holocene sedimentations display strong imprint of basin parameters (mainly water stratification and circulation) in sediment grains and composition. Sediment inputs from the PG catchment led to mixed (in situ biogenic precipitation diluted by detrital supply) sedimentation in the northern part of the PG.

RÉSUMÉ
Sédimentation moderne et holocène dans le golfe Persique.
Le golfe Persique (PG), une mer marginale peu profonde située au nord-ouest de l'océan Indien, est soumis à des conditions environnementales extrêmes (températures et salinité élevées de l'eau de mer) qui influencent la sédimentation du fond. Pour déchiffrer les paramètres contrôlant la sédimentation dans l'environnement du PG, nous avons analysé un total de 25 sédiments de surface, trois carottes courtes, 22 sédiments côtiers, ainsi que les propriétés de la colonne d'eau (température, salinité, oxygène dissous) et l'hydrodynamique (vitesse et direction du courant). Nous avons effectué des analyses sédimentologiques (granulométrie et type de fractions sédimentaires), minéralogiques (lames minces, SEM/EDS, XRD, plaques polies) et géochimiques (scan XRF des carottes). Les sédiments sont principalement composés de silt, mais la fraction de sable peut atteindre environ 80% et l'argile jusqu'à 10%. Le carbonate de calcium et les matières organiques représentent respectivement jusqu'à 18% et 52% des sédiments. Les sédiments de surface du fond marin varient en différentes fractions, toujours avec une quantité élevée de carbonates. Les carbonates détritiques et les minéraux aluminosilicatés sont plus fréquents sur les plages et autour des îles aux roches mères exposées. La carotte qui couvre la sédimentation dans le golfe Persique depuis la fin de l'Holocène inférieur comprend des faciès représentant une signature carbonatée biogénique plus élevée à la base, suivie de plus de matière détritique et organique au milieu. Les variations du niveau de la mer sont interprétées comme le principal moteur de ces variations sédimentologiques : les périodes de niveau élevé ont favorisé les conditions d'eau stagnante et la stratification, permettant ainsi une incorporation plus élevée de matière organique dans les grains enrobés. Les sédimentations récentes montrent une forte empreinte des paramètres du bassin (principalement la stratification et la circulation de l'eau) dans les grains et la composition des sédiments. Les apports de sédiments provenant du bassin versant du PG ont conduit à une sédimentation mixte (précipitations biogéniques *in situ* diluées par un apport détritique) dans la partie nord du PG.

MOTS CLÉS
Golfe Persique,
sédimentation,
carbonate,
hypoxie,
changement climatique.

INTRODUCTION

The Persian Gulf (PG) is a shallow, semi-enclosed basin in the northwest Indian Ocean. It is located at the heart of the global desert belt in an arid/hyperarid climate. The PG experiences an unprecedented dust emission and temperature increase (20% of world dust mission is in this area, air temperature rise is twice the global average), which makes it a potential model for studying the effects of future climate change on other water bodies (Pous *et al.* 2015; Saleh Abolfazl *et al.* 2021; Zittis *et al.* 2022). The basin exhibits a relatively fast general water circulation, which is mainly driven by a high rate of evaporation (Pous *et al.* 2015). Meanwhile, the coastal areas, especially the southern coast of the PG along the Arabian Peninsula, undergo a shallow water carbonate precipitation (Shinn 1973; Wagner & Van der Togt 1973). The bottom morphology inherited from long geological history of compression processes between Arabian and Eurasian plates while sedimentary and hydroclimatic processes exert secondary impacts on shaping the basin (Kennett & Kennett 2007; Orang *et al.* 2018). The PG receives terrigenous sediment from fluvial systems that mainly originate from the northern part. These systems carry sediment from the Zagros and Taurus mountains(Garzanti *et al.* 2016). In addition to the fluvial systems, eolian deposits with annual 89 million ton are a significant component of terrigenous sediments that are mainly supplied from the surrounding deserts by prevailing winds (Kukal & Saadallah 1973; Al-Dousari *et al.* 2017; Ghafarian *et al.* 2022).

The modern sedimentary processes of the PG have been studied by several scholars, mainly for coastal urban development e.g., Hassan (2018), oil and gas explorations e.g., Warren (2010) and environmental purposes (e.g., Houbolt 1957; Sugden 1963; Evans *et al.* 1969; Kendall & Skipwith 1969). However, these studies are scarcer in the northern part of the PG, where detrital sedimentation is more common. Hamzeh (2021) reported that the surface sediment properties in the northern PG are affected by the strong bottom current forcing, terrigenous sediment supply, bottom topography and climate. The sedimentation in the northern part of the PG is dominated by terrigenous material, which gradually changes to carbonate precipitation in the southern coast. The grain size also increases from north to south (Baltzer & Purser 1990), which contradicts the classical depth-related

sediment distribution pattern. The northern part is closer to the Zagros Mountains hydrological drainage and has a mixed sedimentation due to the relatively deeper sub-basin, more fluvial supply and less carbonate sedimentation which is more evident in the silt fraction (Seibold *et al.* 1973).

Despite the importance of the PG as a classic ramp system for carbonate precipitation during the Holocene (Gischler & Lomando 2005), there are still very few studies covering this period: Purser (1973) described the carbonate sedimentation and diagenesis, while (Uchupi *et al.* 1996, 1999) mostly focused on restricted coastal areas. In the absence of paleoenvironmental studies, the reconstruction of the Holocene evolution of the PG basin is still only based on geophysical models (Lambeck 1996).

Climate change is expected to alter sedimentation rates and sedimentary processes in various water bodies. For example, in warm arid climates (e.g., the PG), increased eolian sedimentation and consequently higher bioproductivity are anticipated (Beni *et al.* 2021). This situation could lead to greater preservation of organic matter and a more stable water column (Mahowald *et al.* 1999; Kars *et al.* 2017). To monitor these changes, it is important to study the sediments of the coastal and offshore areas. The Iranian National Institute for Oceanography and Atmospheric Science (INIOAS) has been carrying out regular oceanographic expeditions since 2012 to measure the water properties and the possible changes in the sediment properties in the northern part of the PG. To identify any changes in sediment properties during the industrial period, we need to compare the surface sediments with the pre-industrial ones. For this purpose, we have collected a series of short sediment cores from different sub-basins of the PG. In this study, we have three objectives: 1) to present the offshore sediment distribution pattern and their provenance using sedimentary analyses on surface sediment samples; 2) to detect changes in sediment properties by comparing the surface sediments with Holocene deposits along the cores; and 3) to examine any relationship between the water properties and sediment distribution pattern using physical oceanography and hydrodynamic data obtained by INIOAS expeditions.

STUDY SITE

Geography and geomorphology

The PG is an epicontinental sea of the northwestern Indian Ocean, which extends longitudinally for about 1000 km with a maximum width of 350 km. It has an average depth of 40 m and a maximum depth of 180 m near the northern shores (Ghazban 2009; Pous *et al.* 2013). It has an asymmetric morphology along its longitudinal axis, with a steep slope on the northern shore adjacent to the Zagros Mountains and a gentle slope on the southern and northwestern parts, belonging to the Arabian Peninsula. Seibold & Vollbrecht (1969) divided the basin into six sub-basins: the Mesopotamian shallow shelf at the westernmost head, the Arabian shallow shelf at the south, the western sub-basin and the central sub-basin. The central swell separates the western sub-basin from the central one, and the eastern swell separates the central sub-basin from the Strait of Hormuz (Fig. 1B).

The PG is a shallow marginal sea that has been flooded several times during the Quaternary due to the eustatic sea level changes (Lokier *et al.* 2015; Naderi *et al.* 2024). However, the tectonic setting of the basin has also significantly affected its accommodation space and the rate of flooding over geological time (Konyuhov & Maleki 2006). The main sources of freshwater for the PG are the Zagros and Taurus Mountains, which mainly supply water to the Mesopotamian Shallow Shelf. The Mesopotamian river system consists of the Euphrates and Tigris rivers, which join in the southern Mesopotamian plain and form the Shatt al-Arab River. This river also receives water and sediment from the Karun River before discharging into the northwestern PG (Fig. 1). The Tigris and Euphrates rivers originate in southern Turkey in the Taurus Mountains, flowing through Syria and Iraq before converging in southern Iraq to form the Shatt al-Arab River. The Tigris River has a catchment area of 472 000 km², spanning Turkey, Syria, Iraq, and Iran, with a length of 1 718 km. The mean river discharge was 815 m³/s during 1931-2006, which reduced to approximately 100 m³/s before joining the Shatt al-Arab. The Euphrates River has a catchment area of 444 000 km² and a length of 2 718 km, draining regions in Turkey, Syria, Iraq, and Saudi Arabia. The mean water discharge during 1930-1999 was 559 m³/s, which decreased to 153 m³/s. High discharge typically occurs in April and May, while low discharge is observed in August and July (Saleh D. K. 2010; Al-Ansari *et al.* 2015).

Two rivers from Iran, the Karun and Karkheh, also join the Shatt al-Arab, both originating from the Zagros Mountains. The catchment areas and lengths of the Karun and Karkheh are 72 000 km² and 51 000 km², and 867 km and 964 km, respectively. The water discharge of the Karun River is 777 m³/s, and that of the Karkheh River is 184 m³/s (UN-ESCWA & BGR 2013). The Karkheh River joins the marshlands on the eastern side of the Shatt al-Arab, while the Karun River bifurcates into two channels, one joining the Shatt al-Arab and the other flowing directly into the PG. The average annual sediment discharge of the Karun River is 45 million tons (Najafpour *et al.* 2016).

Extensive construction of dams and hydraulic structures has altered the water and sediment discharge regimes downstream of the Shatt al-Arab's main tributaries (Tigris, Euphrates, Karun, and Karkheh rivers), resulting in reduced discharge and a smoothed annual hydrograph. The Mediterranean climate dominates the catchment area, characterized by hot, dry summers and wet, cold winters. Snowmelt and rainfall determine peak discharge during April-May, accounting for half of the total discharge. Approximately 90% of sediments are supplied from the Anatolian and Zagros mountain belts (Al-Ansari *et al.* 2015; Garzanti *et al.* 2016; Najafpour *et al.* 2016). The Shatt al-Arab is a 192 km long river flowing along the Iran-Iraq border to the northern PG. Several rivers draining from the southern flank of the Zagros Mountains flow directly into the PG, collectively contributing an annual water discharge of approximately 3.5 km³

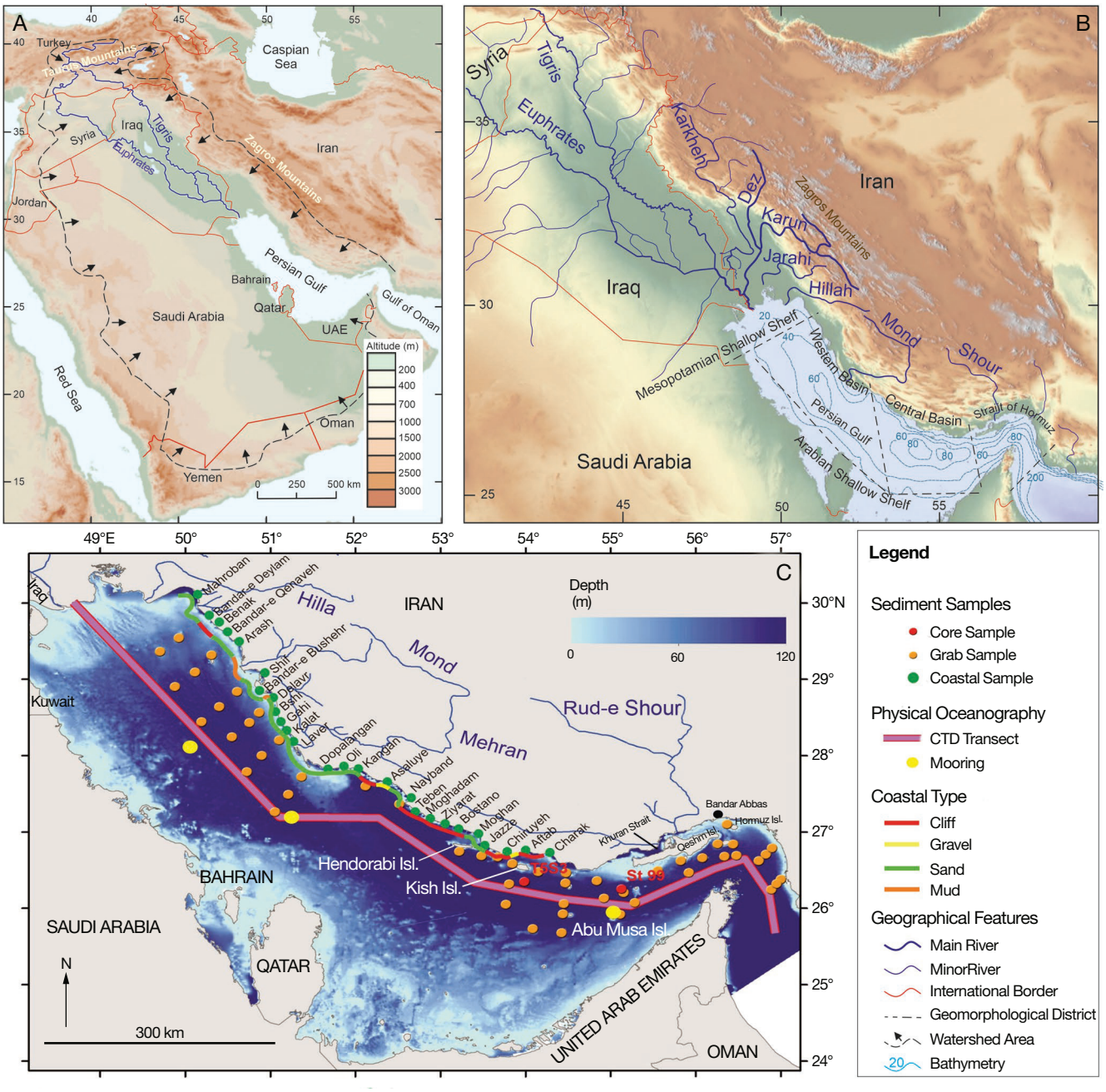

FIG. 1. — **A**, Overall view of the Persian Gulf and surrounding areas; **B**, main rivers flowing into the Persian Gulf and subdivision of the Persian Gulf basin based on the bathymetric characteristics; **C**, location of surficial samples and studied cores, CTD profiling path and current meter stations.

CLIMATE

Climate of the PG is arid to hyperarid with average annual precipitation of *c.* 100 mm and evaporation of 2000 mm (Pous *et al.* 2013). The precipitation increases from south to north and along the Iranian coast reaching to annual average of 225 mm, maximum 324 mm and minimum 110 mm (Beni *et al.* 2021).

The Shamal wind (Arabic for "north") is a strong north-northwesterly wind that varies by season and driver. In summer (June-July), it results from the pressure difference between a temporal high-pressure system over the Arabian Peninsula and a thermal low-pressure system mainly over Iran. These systems and the position of the intertropical convergence zone (ITCZ) affect the wind's onset, duration, and direction. This hot and dry wind affects only the west of the PG, where it carries dust from the deserts of Levant and Iraq. In winter (January-February), it is mainly driven by the Siberian High pressure system, which pushes cold air southward. The Zagros Mountains channel this air towards the warmer PG, creating strong waves in the central basin (Kamranzad *et al.* 2013). Besides the Shamal wind, other regional winds such as southerly Ghows blow over the PG bringing high humidity to the north coast. These winds arise from the interaction of the region's major climatic systems, the Indian Ocean Monsoon (IOM) and the Mid-latitude Westerlies (MLW).

Sedimentology

The Taurus and Zagros Mountains are major sources of sediments fluvial systems of Tigris, Euphrates, and Karun rivers which make Shatt el Arab River entering from northwest into the PG. During the Quaternary glacial periods, the sea level was lower and the rivers were flowing on the exposed basin of the PG, entering to the Gulf of Oman through Strait of Hormoz. The Tigris River sediments have four different sources, three of which are related to basaltic, granitic, and metamorphic rocks from the Taurus Mountains and the fourth belongs to Zagros carbonate formations (Awadh *et al.* 2011; Garzanti *et al.* 2016). The sediments of Shatt el Arab have a similar composition to the Tigris River's sediments (Philip 1968). The Zagros Mountains is a major source of weathered carbonate, marl, sandstone and conglomerate (Aghajari and Bakhtiari Formations) as well as weathered ophiolitic rocks into the northern PG (Berry *et al.* 1970; Purser & Seibold 1973; Moghadam & Stern 2011; Sahraeyan 2013).

The sedimentation rate varies between *c.* 0.1 and 5 mm in the PG, depending on the geomorphological and geographic position (Al-Ghadban *et al.* 1998). Sedimentation rate has also changed over time; during the Late Holocene, the range varied between 0.13 and 0.74 mm.yr^{-1} in the Strait of Hormuz and from 0.18 to 2 mm.yr^{-1} in the central basin (Al-Ghadban *et al.* 1998). According to these studies the area of interest (Core St 99) has a rough estimation of 0.15 mm. yr^{-1} during the Holocene (Hamzeh *et al.* 2021), indicating that the base of the cores could reach to the Early Holocene (>7500 *c.* yr BP). The highest sedimentation rates occurred at the northwest coasts of the PG where several ephemeral rivers flow into the gentle coastal slopes and marshlands (Hamzeh & Lahijani 2022) (Fig. S1.1). These coastal areas are classified as river- and tide-dominated coasts by Pourkerman *et al.* (2020), where hydrodynamically has lower energy than other parts of the Gulf.

Oceanography

Physical oceanography

The PG exhibits significant annual variations in sea surface temperatures (SST), with monthly mean SST climatologies ranging from 19.6 °C in February to 33.2 °C in August (NOAA 2024). (Fig. S1.2). Additionally, extensive areas of hypersaline water with salinity levels surpassing 42 practical salinity unit (psu) are prevalent. During summer, the greatest disparity in density between the surface and bottom layers occurs e.g., ranging from 23.74 to 27.10 Kg/m^3 (+ 1000) (Azizpour *et al.* 2014; Saleh *et al.* 2021). This difference diminishes notably during the winter season. In the summer months, the thermocline depth is primarily found between depths of 25 and 50 meters, resulting in a water column characterized by two layers (Reynolds 1993). Throughout the summer, the stratification of the water column hinders the swift exchange of deep water due to the weaker Shamal wind and consequent limited vertical mixing, spanning across most of the PG. This stratified condition endures in the central and western sectors until mid-autumn. Conversely, in winter, as the air gradually cools and surface layer temperatures drop, the density of the surface layer increases. This prompts an extension of vertical mixing into the adjacent near-bottom layer that is strengthened by more intensive Shamal wind. The result is a nearly uniform density across the water column in the PG and the Strait of Hormuz starting from January (Saleh *et al.* 2021).

The circulation patterns within the PG are primarily influenced by a reverse-estuarine Mediterranean-type flow. This circulation involves the export of high-density hypersaline PG water (PGW) along the southern edge of the Strait of Hormuz into the Gulf of Oman (Kämpf & Sadrinasab 2006). Simultaneously, a surface inflow of less saline and lower density waters originating from the Indian Ocean Surface Water (IOSW) occurs along the northern side of the strait. This phenomenon has been documented by Chao *et al.* (1992), Reynolds (1993), and Swift & Bower (2003).

In the PG, hypoxia (defined as dissolved oxygen (DO) levels less than 2 mg.l^{-1}, or 61 µmol.kg^{-1}) from summer to autumn appears to be a recurring event, primarily occurring at depths of ≥ 50 meters down to the seafloor. This seasonal hypoxia initiates in late summer and reaches its peak severity during mid-autumn, covering an area of up to 50 000 km^2 within the PG (Saleh *et al.* 2021). In the Strait of Hormuz, seasonal hypoxia likely emerges in early summer, particularly in the lowermost part of the eastern region on the Iranian side. This area is less influenced by the high-salinity outflow of water from the PG (Saleh *et al.* 2021). Within the hypoxic and low-oxygen zones, researchers discovered elevated levels of phosphate and nitrate concentrations, along with low pH values (Al-Ansari *et al.* 2015; Saleh *et al.* 2021). These findings indicate the substantial generation of nutrients and dissolved inorganic carbon through the decomposition and remineralization of submerged organic material in layers beneath the thermocline. The observed reduced pH values in the hypoxic waters of the PG reached levels comparable to the predictions for the surface ocean by the year 2100 under the conditions of ocean acidification (Saleh *et al.* 2021). Lachkar *et al.* (2022) undertook the task of reconstructing the dissolved oxygen trends within the PG from 1982 to 2010 and investigating the underlying factors governing these changes. Their research uncovered a notable decline in oxygen levels across the study period. The oxygen content witnessed a decrease of almost 1% per decade, while the near-bottom oxygen concentration dwindled by 10 to 30 mmol.m^{-3} in the deeper regions of the PG from the early 1980s to the late 2000s.

Hydrodynamics

The general water circulation in the PG is related to the excess evaporation from the PG surface, which causes an influx of less saline Indian Ocean Surface Water (IOSW) through the northern parts of the Strait of Hormuz and the formation of dense water on the northwest part of the PG and Arabian shallow shelf as a reverse estuary (Kämpf & Sadrinasab 2006). The water circulation is also influenced by winds, tides, and riverine freshwater influx, among which tidal currents have the greatest role in energy of water motion (Reynolds 1993; Pous *et al.* 2015). Different currents have a different time scale: tides vary at diurnal or semi-diurnal periods; wind driven

currents develop over some days; and density-driven currents change weekly or seasonally (Reynolds 1993). The PG is a shallow sea and wind-driven currents have substantial role in generating currents in the whole basin. Density-driven, tidal, and wind-driven currents seem to play an important role in sediment transport (Li *et al.* 2015). Tidal currents disturb and mobilize sediments and residual and density-driven currents transport them. Previous studies of current dynamics in the PG and the Strait of Hormuz (Reynolds 1993; Johns *et al.* 2003; Azizpour *et al.* 2016) show that tidal currents are dominant in this area, followed by wind-driven and density-driven currents. Fig. S1.3 shows the current speed for a station near the Abu-Musa Island in the PG and the prominent role of tidal current. The current speed increases from west to east(Johns *et al.* 2003; Azizpour *et al.* 2016). The mean speed of residual (or density-driven) current is about 30 cms^{-1} (Figs S1.3-S1.6).

MATERIAL AND METHODS

A total of 50 surface sediment samples and two sediment cores from the PG obtained during the PGE-19 oceanographic expedition in 2019 by the Iranian National Institute for Oceanography and Atmospheric Science (INIOAS) (Fig. 1C) using VanVeen grab sampler and gravity corer, respectively. Moreover, 26 surficial coastal sediment samples have been collected using a shovel along the northern coast of the PG (Fig. 1C).

Magnetic susceptibility (MS) of the cores was measured at the INIOAS laboratory using a Bartington Magnetic Susceptibility Meter MS2C in two cm interval and high variability of data normalized regarding the mean value of each core. XRF scanning has been done on one core using an ITRAX core scanner at CEREGE laboratory, Aix- Marseille University.

A total of 223 sediment sub-samples from the cores, marine surface samples and coastal samples have been analysed for sedimentological investigation (Table 1). Prior to the sample treatments, all the samples were oven dried at 60°C. Grain size, calcium carbonate, and OM contents were measured for all the samples. The large biogenic carbonate removed and organic matter-free sediment samples were granulometrically characterised by standard sieving a Laser-Particle-Sizer (Fritsch Analysette Comfort 22, analysing range of 0.04 to 2000 µm). Calcium carbonate content was determined using a Bernard calcimeter and expressed as dry sediment weight. The OM content was measured by wet digestion through oxidation in hydrogen peroxide on bulk samples (Schumacher 2002).

For the fauna identification, 100 sub-samples were examined firstly for macrofauna and then they were wet sieved using a mesh size of 125 µm and dried to study under the optical microscope. Scanning Electron Microscope (SEM) and Energy Dispersive Spectroscopy (EDS) of Geological Survey of Iran (GSI) were utilized for 10 samples to identify sediment grain analysis and diagenesis. As the majority of the marine samples are fine-grained sediment, therefore the mineralogical identifications were based on XRD analysis on 21 representative bulk samples and clay mineralogy. Analysis of the XRD has been done in Kanpazhuh Co. Lab. Finally, the sand fraction was studied optically using Zeiss Axio Lab microscope. Twenty sediment blocks were preserved in epoxy resin. Fifteen of which were mounted on thin sections. We focused our analysis on the lithoclasts. A total of 1750 lithoclasts have been classified. Moreover, five sub-samples were prepared for polish section to be studied using reflective polarizing microscope. The polish sections and thin sections were prepared at the laboratory of Faculty of Geology, University of Tehran.

RESULTS

Surface sediments

Grain size

The distribution of surface sediments shows that coarse-grained sediments of gravel and sand are mainly accumulated in the middle part of the PG. Clay contributes less than ten percent (average 2.5%) of the surface sediments content (Figs 2; S2.1). The surface sediments in the northwestern part of the PG are mainly composed of medium silt to medium sand. The surface sediments in the northwestern part of the PG have similar amounts of sand and silt (48% and 47%, respectively), and a low percentage of clay (about 11%).

The sediments near the north-eastern Iranian shores are mostly composed of fine to medium silt, which becomes coarser towards the deeper part. Silt is the dominant sediment fraction, making up about 80% of grains. Sand is a minor component, with less than 20%. However, fine sand becomes more abundant near the seasonal and permanent rivers (such as Hilla, Mand and Mehran) (Figs 2; S2.1). The sediment composition changes to gravelly sand in deeper parts of the Strait of Hormuz. The gravel component consists mostly of shell debris, which has the highest proportion near Ras-e Motaf in the west and Hendorabi Island in the East (Figs 2; S2.1). Sand is the main sediment fraction in this area, and it is often in very coarse class. The sand portions have two different sources: shell fragments in the West and East of the PG up to 86%, and ooid particles in the central basin. The sediments get coarser in the eastern part of the Strait of Hormuz.

The sediment grain size in Khuran mangrove forests is mainly fine silt and sand (Figs 2; S1.1). The sediment becomes finer in the middle parts of the Qeshm mangrove forests. However, the banks of Khamir and the Mehran River delta have coarser-grained sediment of sandy silt and silty sand. The distribution of sediments on the (Folk 1980) ternary diagrams (Fig. S2.2) shows that most of the surface sediments are silt and sandy silt (Fig. 2). The northern coasts of the PG have sandy-gravelly sediment, which changes to rocky shores in some parts of the north PG coast. Muddy shores are found in low-energy environments in the northwestern PG (Figs 2; S2.1).

Organic matter

The amount of OM in surface sediments varies from 5% to 18%. The highest abundance of OM has been observed in

TABLE 1. — Sampling locations in this research, and analysis applied for them. For the surface samples in the Persian Gulf and water measurements only shown in the Figure 1C.

Environment	ID	Coordinates (X, Y)	Depth (m)	Thin section	XRD	SEM	Polish section
Coastal	Mogham	26°58'11"N, 53°28'11"E		×	–	–	–
	Ziarat	27°6'0"N, 53°5'24"E		×	–	–	–
	Kalat	28°23'59"N, 51°8'59"E		×	–	–	–
	Delvar	28°45'0"N, 51°2'59"E		×	–	–	–
	Kangan	27°49'47"N, 52°2'59"E		×	–	–	–
	Bustanu	27°7'12"N, 53°1'48"E		×	–	–	–
	Kuhestak	27°7'47"N, 56°6'0"E		×	–	–	×
	Asaluye	27°38'59"N, 52°22'11"E		×	–	–	–
	Oli	27°50'23"N, 51°52'48"E		×	–	–	–
	Aftab	26°43'48"N, 53°57'0"E		×	×	–	×
	Khun Sorkh	27°7'47"N, 56°6'0"E		×	–	–	×
	Dopalangan	27°50'23"N, 51°39'35"E		×	–	–	×
	Homeiran	26°41'59"N, 55°6'0"E		×	×	–	×
	Bashi	28°40'47"N, 51°4'12"E		×	–	–	–
	Kong	26°34'47"N, 54°55'47"E		×	–	–	×
	Charak	26°43'48"N, 54°16'12"E		×	×	–	×
	Abomusa	25°53'24"N, 55°1'48"E		×	–	–	–
	Farur	26°19'12"N, 54°31'12"E		×	–	–	–
	Gardaney-e Mogham	27°1'11"N, 53°17'59"E		×	–	–	×
	Laver	28°15'0"N, 51°16'12"E		×	–	–	×
	Moallem	26°38'24"N, 55°2'23"E		×	×	–	×
	Kish	26°33'0"N, 54°1'12"E		×	–	–	–
Marine (Grab)	104	25°40'47"N, 54°25'12"E	–59	×	–	–	–
	90	26°19'12"N, 53°48'36"E	–90	×	–	×	–
	J	26°5'23"N, 54°5'24"E	–84	×	–	–	–
	121	26°50'23"N, 56°15'35"E	–49	×	×	×	–
	116	26°37'12"N, 55°49'12"E	–34	×	–	–	–
	114	26°4'12"N, 55°17'23"E	–86	×	–	–	–
	G	26°44'23"N, 53°13'11"E	–83	×	×	×	–
	TS	26°11'59"N, 55°9'35"E	–107	×	–	–	–
	64	27°15'36"N, 51°3'36"E	–69	×	×	–	–
	62	27°29'23"N, 51°12'36"E	–74	×	–	–	–
	54	28°0'0"N, 50°53'59"E	–61	×	×	–	–
	28	29°5'23"N, 50°6'35"E	–42	×	×	–	–
	30	28°53'59"N, 49°52'48"E	–44	×	–	–	–
	56	27°48'0"N, 50°42'0"E	–65	×	–	–	–
	42	28°38'24"N, 50°23'59"E	–49	×	×	–	–
	88	26°34'47"N, 53°51'0"E	–54	×	–	–	–
	84	26°41'24"N, 53°28'47"E	–58	×	×	–	–
	44	28°26'24"N, 50°11'23"E	–55	×	–	–	–
	51	28°14'23"N, 50°32'59"E	–60	×	–	–	–
	118	26°27'36"N, 55°55'12"E	–59	×	×	–	–
	123	26°40'47"N, 56°20'24"E	–71	×	–	–	–
	D	25°43'48"N, 53°5'24"E	–64	–	×	–	–
	92	26°3'0"N, 53°46'12"E	–75	–	×	–	–
	108	26°7'47"N, 54°55'12"E	–82	×	×	–	–
	26	29°19'12"N, 50°18'36"E	–27	×	–	–	–
Core T5s4	9-11	26°4'47"N, 53°46'12"E	–74	×	–	–	–
	15-17			×	×	–	–
	19-21			×	–	–	–
	21-23			×	–	–	–
	25-27			–	×	–	–
	29-31			–	×	–	–
	31-33			×	–	–	–
Core T5s3(2)	13-15	26°21'0"N, 53°48'36"E	–86	–	×	–	–
	31-33			–	–	–	–
	59-61			–	×	–	–
	81-83			–	×	–	–
Core St99	67-69	26°30'0"N, 55°17'59"E	–75	–	–	×	–
	101-103			–	–	×	–

the west of the PG, south of Qeshm Island and east of Kish Island. The lowest values of OM are in the areas of Lawan, Hendorabi, and Abu Musa islands (Fig. S2.1A).

Calcium carbonate

The calcium carbonate content varies from 12% to 52% in surface sediments. The highest values of calcium carbonate are

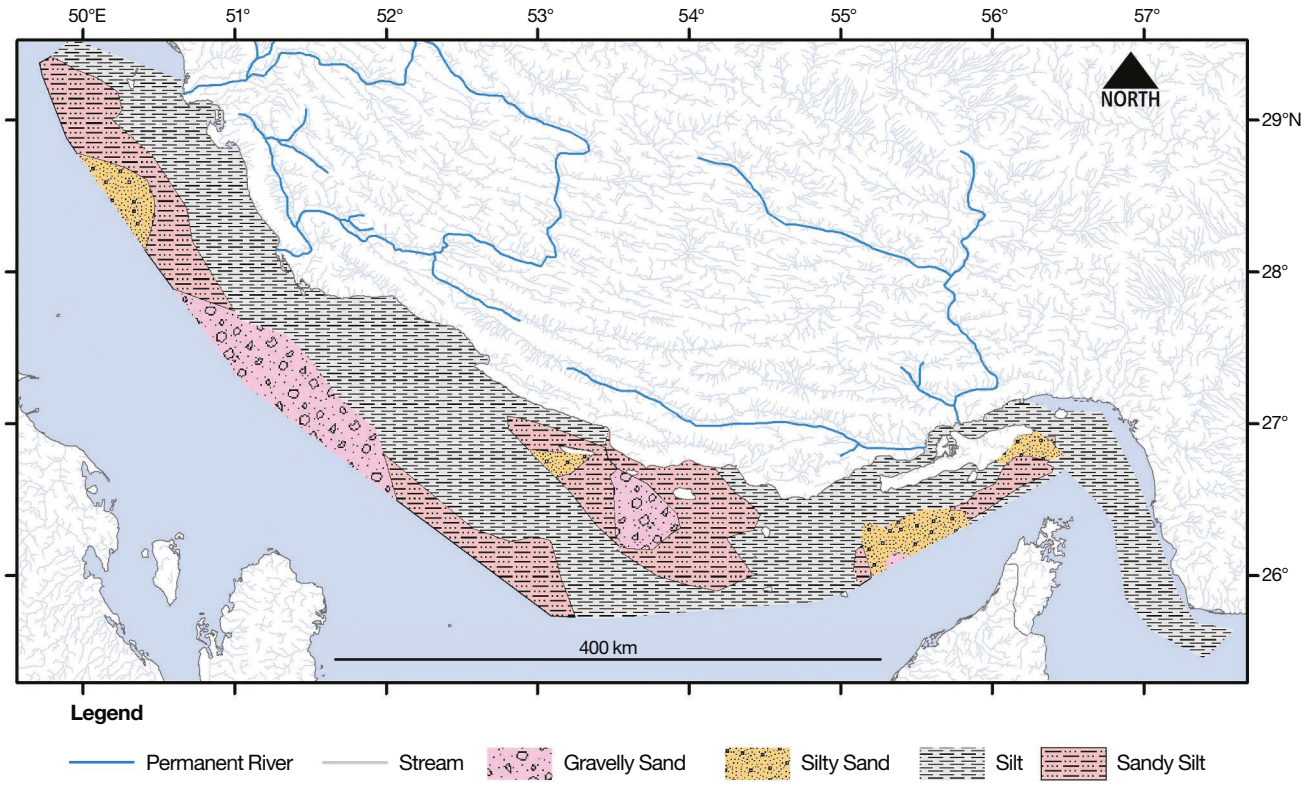

FIG. 2. — Surficial sediment grain size in the northern Persian Gulf.

observed around the islands of Kish, Hendorabi, Lawan and also in the southern parts of Abu Musa Island. On the other hand, the lowest values of calcium carbonate are observed in nearshore areas of the western coasts, Hormuz Island and east and northeast of the Strait of Hormuz (Fig. S2.1A).

Mineralogy

In the clayey part of the PG surface sediments, the dominant minerals are kaolinite, aragonite and calcite. Their amount includes up to 89% of the minerals identified in XRD. After them, muscovite and quartz are found in the samples up to 14% and 8.5%, respectively. The amount of quartz and muscovite is higher towards northwest of the PG, while the samples that were collected in the northeast of the PG and near Qeshm Island have more kaolinite. The highest amount of calcium carbonate (calcite and aragonite) was seen in the surface samples of the middle part of the PG (surface sample 64% with 69.5% carbonate) (Table 2; Figs S2, S3). The dominant minerals in the fine-grained part of the coastal sediments include aragonite and calcite, the total amount of which varies from 32% to 59%. After them, quartz with a maximum of 20% and kaolinite with a maximum of 33% are present in some samples.

Studies of thin sections of coastal surface samples reveal the most important mineralogical changes in diopside and zircon minerals. The highest abundance of diopside has been observed in Aftab, Duplangan and Hamira stations. Zircon has been observed only in Doplangan and Farur stations (Figs 3; S4).

Also, we observed a high amount of ooid and rock fragments, which are more abundant in Doplangan, Kohestak, Moalem, Kong, Bashi, Oli, Delwar and Kalat beaches. These particles are more available in the clastic beaches while they are absent in carbonate beaches of Kish and Farur islands. In most ooids, we have observed signs of calcite substitution instead of aragonite and destruction of layering in the ooids (Figs 3; S4).

The main components of polished sections of beach samples include siliciclastic particles. Iron oxides and hydroxides (ilmenite, hematite and magnetite) and pyrite are very small amount of the constituent minerals of these samples. The heavy minerals in the samples do not show much diversity.

Coarse sand and gravel portions existed in the northern part of the PG are generally made of gray to black coated grains. Results of thin sections and SEM-EDS analysis are demonstrated that coated grains have two different origins. The first one is coated shells and the second made of coating around a nuclei (ooid). According to the EDS analysis the coating material made of kaolinite and organic materials (Figs 4; S5).

CORE ANALYSIS

Core St 99

The analysis of sediment constituents by XRF core scanning shows numerous changes and fluctuations along the core (Figs 5; S6.1). Calcium and strontium, which contribute more to carbonate structure show a similar trend along the cores. Both Ca and Sr have elevated value in the basal part of the core. General trend of Fe, Mn and Ti are similar and they display minimum in the basal core that are opposite

TABLE 2. — Percentage of mineral content in the studied samples. In the middle part of the table that related to cores, numbers denote the depth of subsampling from top in cm.

ID	Ankerite	Aragonite	Augite	Calcite	Diopside	Dolomite	Magnesite	Monetite	Mordenite	Pumpellyite	Quartz	Mg calcite	Kaolinite	Muscovite	Microcline	Aegirine	Clinozoisite	Plagioclase	Polyhalite	Chalcopyrite	Dickite	Nepheline	Smectite	Halite	Nontronite	Nitratine	Kainite	Chlorite	Anorthite	Tobermorite	Epidote	Albite	Chromite	Hornblende	Carnallite	Chalcocite	Lepidolite
Charak	7	7	–	33	–	4	–	–	–	–	–	15	33	–	–	–	–	–	–	–	–	–	–	–	–	–	–	–	–	–	–	–	–	–	–	–	–
Aftab	9.5	6.7	4.2	45.8	1.1	5	2.2	2.4	0.8	3	18.3	–	–	–	–	–	–	–	–	–	–	–	–	–	–	–	–	–	–	–	–	–	–	–	–	–	–
Homeiran	–	6.3	0.9	16.4	2.4	3.4	–	–	–	–	19.8	10.9	30	6.2	3.9	–	–	–	–	–	–	–		–	–	–	–	–	–	–	–	–	–	–	–	–	–
Moallem	–	–	–	59	–	–	–	–	–	–	14.9	–	–	–	–	4.2	8	4.1	6.6	–	–	–		–	–	–	–	–	–	–	–	–	–	–	–	–	–
T5S3 13-15	–	–	–	10.1	–	–	–	–	–	–	3.4	–	54	6.9	–	–	–	–	–	–	1.2	–	2.2	–	–	1.8	–	7.8	–	–	–	–	–	–	–	–	–	–
T5S3 59-61	–	–	–	3.8	–	–	–	–	–	–	4.5	–	45.6	7.2	–	–	–	–	–	–	–	–		–	–	–	–	2.9	–	–	–	–	–	–	–	–	–
T5S3 81-83	–	2.8	–	5.8	–	–	–	–	–	–	–	–	60	13.2	–	–	–	–	–	–	–	–	1.4	–	–	–	–	10.8	–	–	–	–	–	–	–	–	–
T5S4 29-31	–	12	2.2	11.7	–	1.6	–	–	–	–	2.6	13.3	47	–	–	–	–	–	–	0.1	–	–	1.6	–	–	–	–	–	–	–	0.4	–	–	–	–	–
T5S4 25-27	–	15	–	17	–	1.7	–	–	–	–	3	12	50	–	–	–	–	–	–	–	1.3	0.4	1.7	–	1.1	–	0.3	–	–	–	–	–	–	–	–	–	–
T5S4 15-17	–	19.3	–	24.5	–	3.6	–	–	–	–	7.8	13.3	20	–	–	–	–	–	–	0.1	–	–	5.6	1.4	–	–	–	–	–	–	4.2	–	–	–	–	–
28	6.2	12	–	31	–	–	–	–	–	–	5.8	–	27	10	–	–	–	–	–	0.8	0.6	1.3	1	2.3	2	–	–	–	–	–	–	–	–	–	–	–	–
42	–	17	–	45	–	0.7	–	–	–	–	7.5	–	–	14	–	–	–	–	–	0.9	–	1.8	2	2.7	1	1.6	–	–	–	–	–	–	–	–	–	–	–
54	8.4	22.8	10.1	36	–	–	–	–	–	–	–	–	–	12	–	–	–	–	–	–	4	–		–	–	1.6	1.4	–	–	–	–	–	–	–	–	–	–
64	3.1	33.27	–	36.2	–	2.1	–	0.5	–	–	4.6	–	–	5.9	–	–	–	–	–	1.63	–	2.8	0.2	–	–	–	–	4.5	5.2	–	–	–	–	–	–	–	–
84	–	2.9	–	8.4	–	–	–	–	–	–	1.3	–	70.65	12	–	–	–	–	–	0.14	–	2		–	–	–	–	–	–	1.1	1.5	–	–	–	–	–	–
92	–	4.9	3.4	17.8	–	–	–	–	–	–	1.65	4.5	45	8.2	1.7	–	–	–	–	0.2	–	–	3.4	–	–	0.2	–	6.6	–	2.4	–	–	–	–	–	–	–
108	–	23	–	16	–	–	–	–	–	–	3	11	30	7	–	–	–	–	–	0.5	1.8	1.5		–	–	–	–	–	5	–	–	–	–	–	–	–	–
118	–	5	–	10	–	–	–	–	–	–	–	–	64.1	10	–	–	–	–	–	0.5	3	–		–	–	1	–	5	–	1	–	0.2	–	–	–	–	–
121	–	3.8	–	14.6	–	2.3	–	–	–	–	2.2	–	39.17	19	–	–	–	–	–	0.54	6.6	–	0.18	–	–	–	–	–	–	5.4	–	1.9	1.3	0.9	2.1	–	–
D	12.5		–	15.6	–	–	–	–	–	–	2.6	11.9	49	–	–	–	–	–	–	0.29	–	1.4	3.5	–	–	–	–	3.3	–	–	–		–	–	–	–	–
G	–	15	–	5	2.5	–	–	–	–	–	1.1	–	68	1.7	–	–	–	–	–	–	–	1.1		–	–	–	–	2.8	–	–	–		–	–	–	1.3	1.1

of Ca and Sr curves. On the other hand, titanium, iron and manganese are indicator of clastic sediments entering the basin, which show the least biological and chemical participation in situ. MS value shows smooth trend along the core barely could be comparable to the lithogenic elements' curve (Figs 5; S6.1).

Lithoclasts are classified into 12 different groups based on microscopic features and morphological characteristics, which include aggregates, fractures with fresh surfaces, unaltered particles, lawsonite, glaucophane, cylindrical grains, grains with rounded surfaces, compressed grains, marine and mostly fossil cements and coated grains (Fig. S6.2).

The lithoclasts varied in plenty and size along the core, and they were related to the sediment compaction. The base of the core has the highest abundance of lithoclasts, which were mainly composed of coarse marine cements, aggregate material, and lawsonite. The amount of lithoclasts in the studied core significantly decreased toward core top (Fig. 5).

Based on the biological, geochemical, sedimentological properties of the sediments, three main facies can be distinguished in the studied cores (Figs 5; S6.2, S7). According to the sedimentation rate and the sediment properties, it seems that basal core (facies C) has deposited during the Mid-Holocene (*c.* 7500-4200 yr BP). Facies A contains coarse-grained sediments consisting of cemented lithoclasts. SEM-EDS analysis shows that the cement is mainly composed of calcium carbonate. The cement is intermixed with very fine silt and clay minerals, suggesting deposition in a calm and shallow marine environment (Figs 6A; S8). The middle part of the facies, greenish lithoclasts are generally composed of high-magnesium carbonate and organic matter in the matrix of kaolinite (Fig. 6B). Figure 6B-I shows rounded grains without sharp corners, indicating transport in the sedimentary basin.

In this facies, X-ray images show a very dense texture that is accompanied by higher Sr and Cl values. According to the high frequency of planktonic (*Globigerina praebulloides* Blow, 1959*, Orbulina universa* d'Orbigny, 1839*, Neogloboquadrina praehumerosa* (Natori, 1976)*, Globigerinella obesa* (Bolli, 1957), *Globigerinoides sacculifer* (Brady, 1877)) and benthic foraminiferal shells (*Asterorotalia pulchella* (d'Orbigny, 1839) and *Bigenerina aspratilis* Loeblich & Tappan, 1994), the higher calcium and strontium peaks could be explained in this facies.

An increase in the values of iron has been observed at the middle part of this facies that continues to the end of the facies.

Facies B is started by a significant drop of the values of all studied elements, frequency of foraminifera assemblages, and grain size gradually decreased to make fine-grained muddy sediments (Figs 5; S6.2).

The facies C is started with an increase in the Fe and Mn values, and foraminifera frequency. The X-Ray image shows higher density of the sediment. Sedimentological properties are indicated by increase sediment particle size and general decrease of lithoclast abundance. The frequency of planktonic and benthic foraminifera show significant changes along the rest of the facies (Fig. 5). According to the position of the facies C on top of the core, it is certainly attributed to the late Holocene.

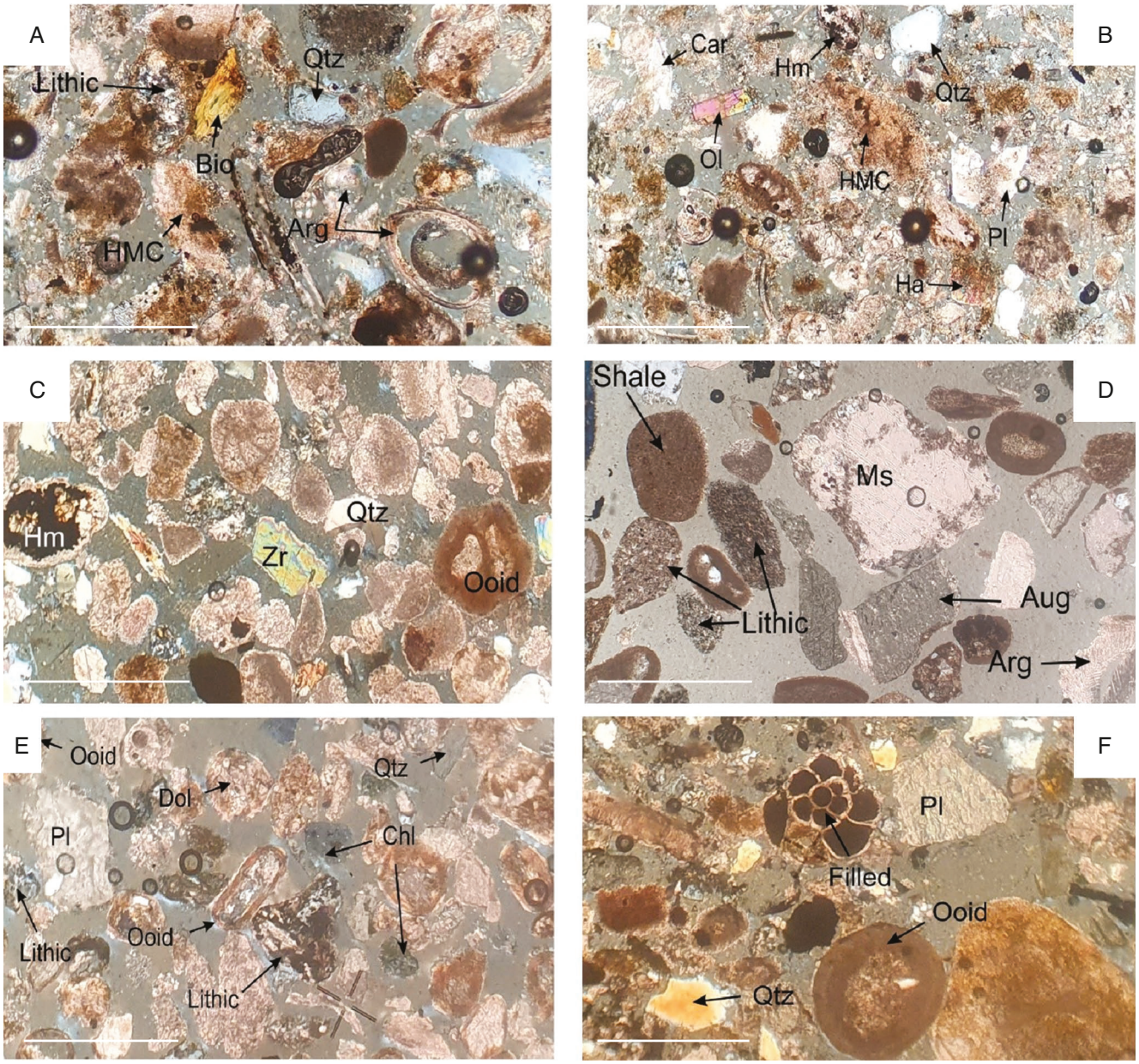

Fig. 3. — Microphotographs in crossed polarized light of: **A**, **B**, T5S3; **C**, Dupalangan; **D**, Homeria; **E**, Kohestak; **F**, Moalem. Abbreviations: **Qtz**, Quartz; **Bio**, biotite; **HMC**, High magnesium calcite; **Arg**, Aragonite; **Car**, Carnallite; **Hm**, Hematite; **Ol**, Olivine; **Pl**, Plagioclase; **Ha**, Halite; **Zr**, Zircon; **MS**, Muscovite; **Aug**, Augite; **Dol**, Dolomite; **Chl**, Chlorite; **Lithic**, lithoclast. Scale bars: 250 µm.

Core T5S3

Core T5S3 has homogenous sandy mud texture from top to base. According to the XRD analysis results, the most abundant minerals in this core are kaolinite, calcite, and aragonite. Muscovite and quartz are also present, but in lower amounts. Moreover, biotite is demonstrated in two horizons of 59-61 cm and 81-83 cm with of 28% and 5% of the counted minerals, respectively. Dolomite exists in some coastal and marine samples at the rate of 1% to 5%. The optical mineralogy studies revealed that the studied horizons contained single olivine and plagioclase grains with hematite pigments (Figs 3; S9).

DISCUSSION

Modern sedimentation environment

Sedimentation in marine environments is controlled by a wide range of intra- and extra-basinal driving factors (Mahiques *et al.* 2004; Garzanti *et al.* 2016; Dauner *et al.* 2022). Basin morphology, hydrodynamics, water column properties and biogechemical processes incorporate in bottom sedimentation. The climate over the catchments basin and sediment supply are also determinant in marine basin sedimentation (Einsele 1996; Jin *et al.* 2020).

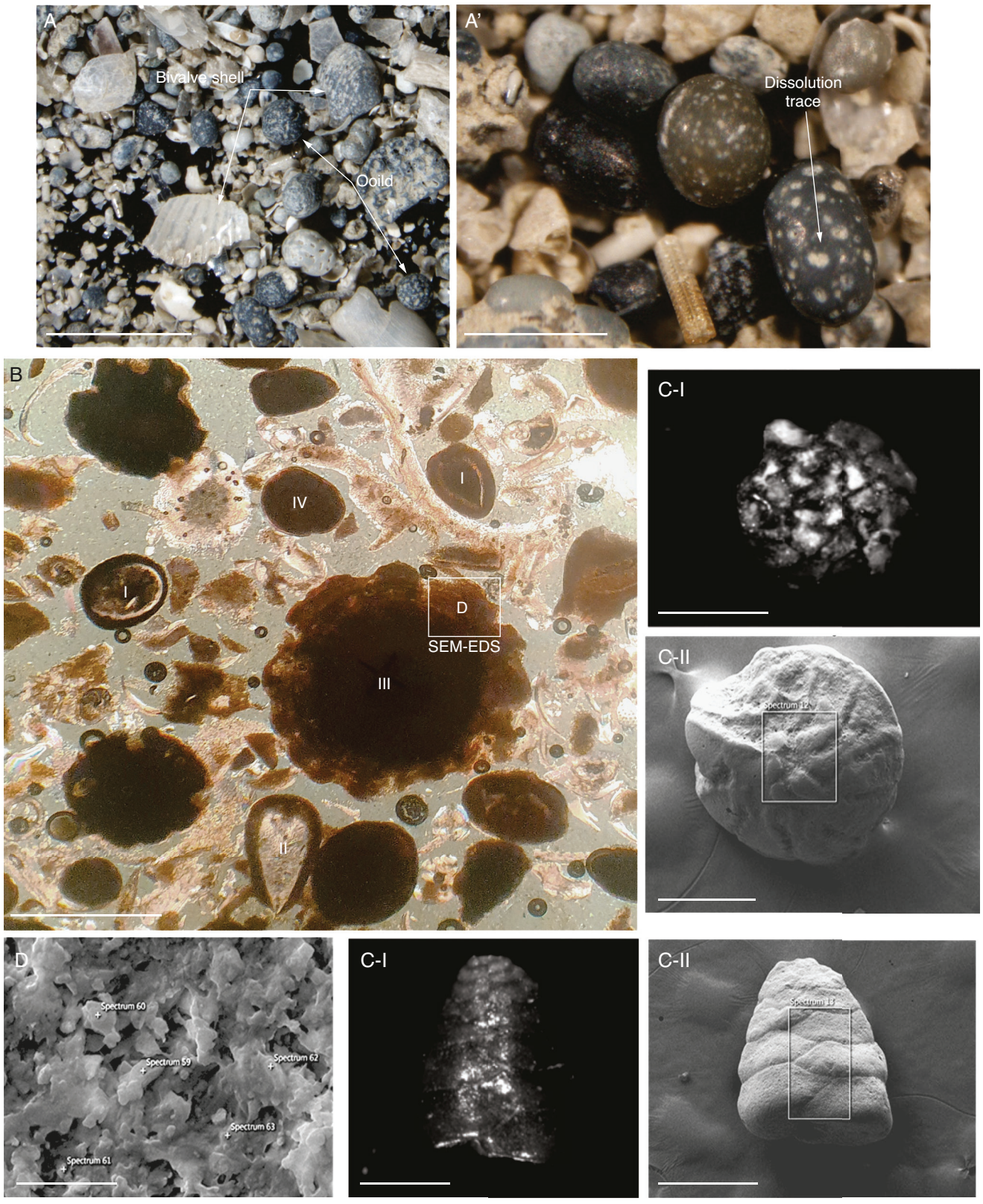

FIG. 4. — **A**, **A'**, Binocular images from coated grains from the central of the Persian Gulf; **B**, microphotographs in crossed polarized light: **I**, coated bioclast filled by kaolinite and organic matter; **II**, coated bivalves shell filled by gypsum and halite; **III**, ooid with dissolved surface; **IV**, pellet; **C**, binocular (**C-I**) and SEM photo (**C-II**) from coated shells in cross-sectional (top) and long-axis (bottom) views; **D**, SEM photo from ooid suggested separated plat of kaolinite covered by organic matter. Scale bars: A, 1 mm; B-D, 250 µm.

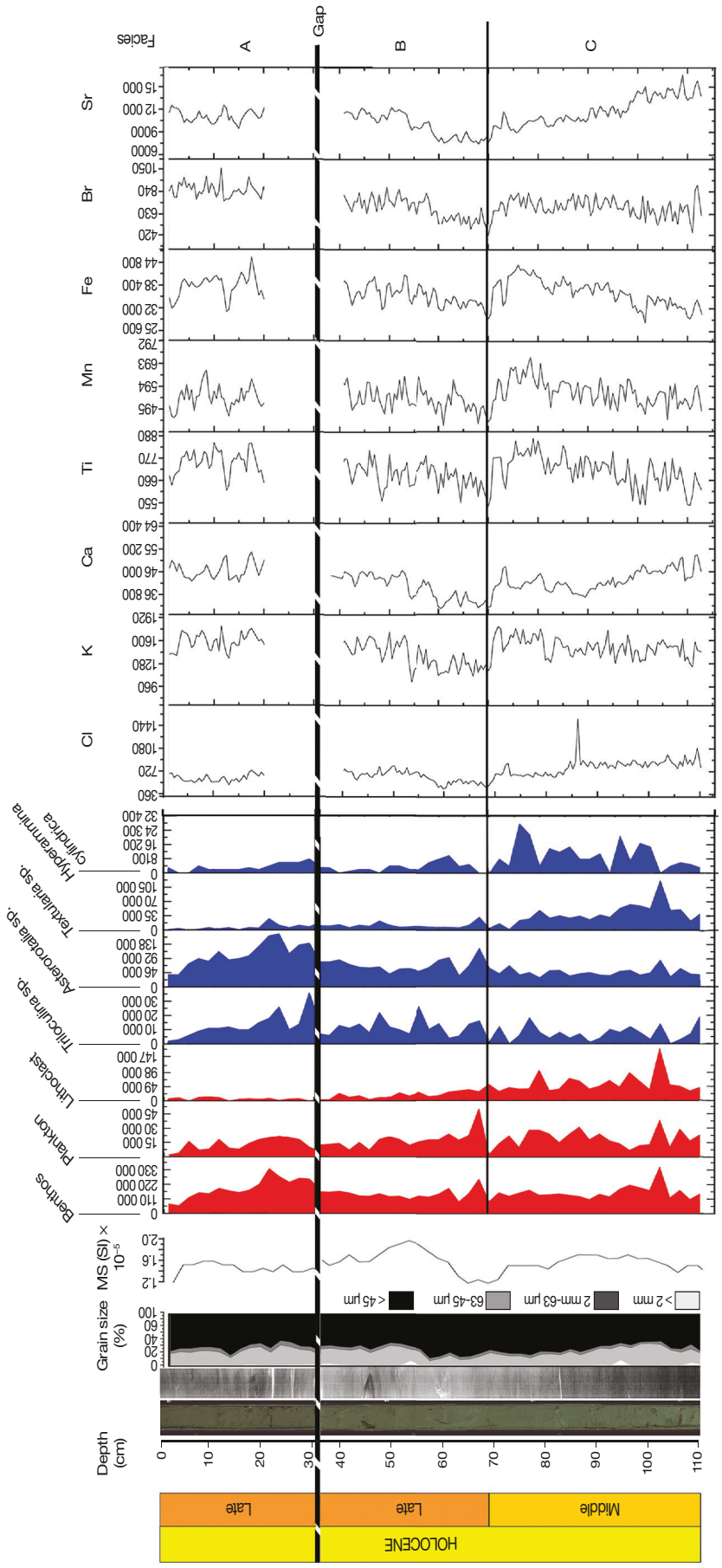

FIG. 5. — X-ray photograph, lithostratigraphy, frequency of total benthic, planktonic and lithoclast in the core St99. The images also represented element changes and main facies at the study core.

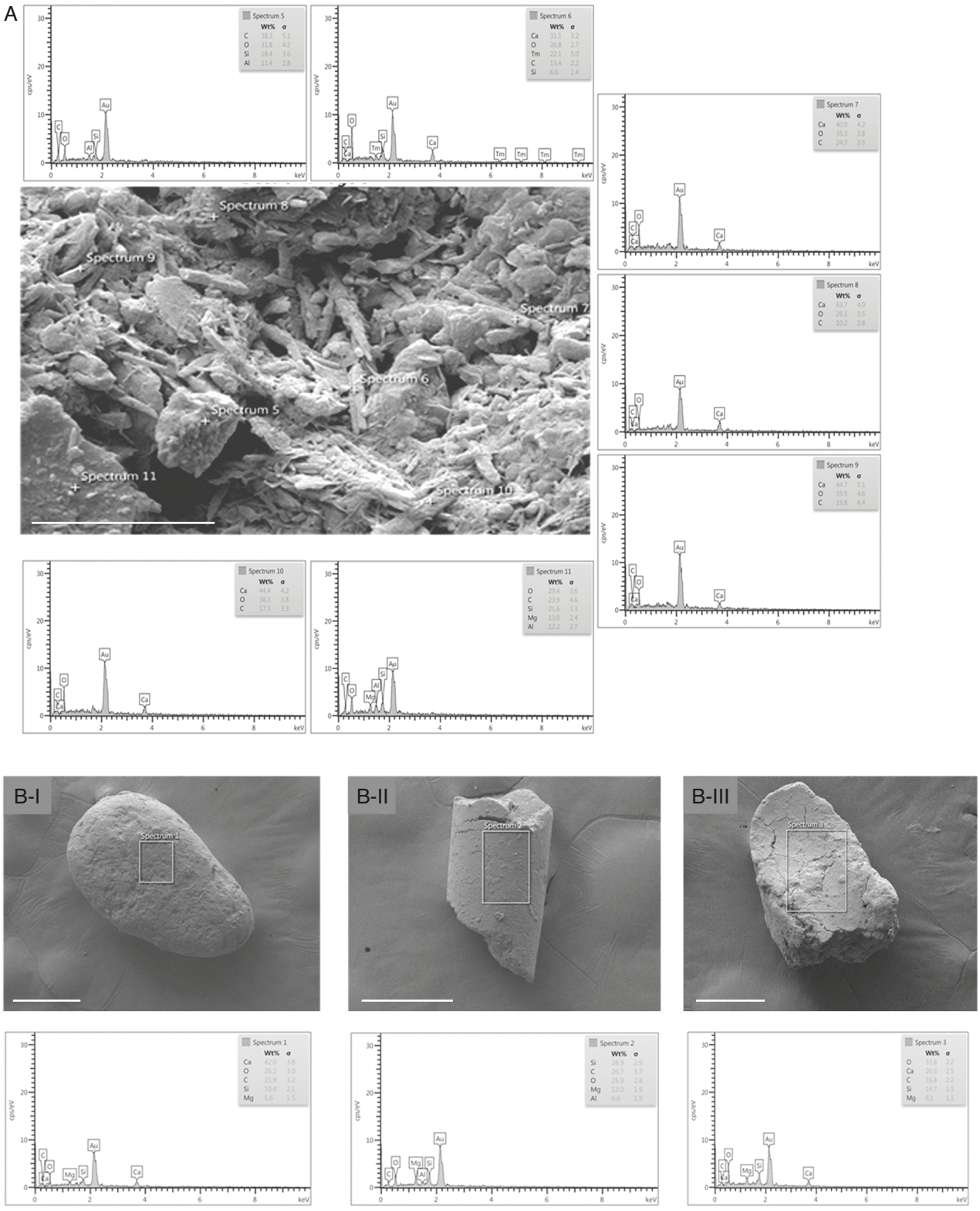

FIG. 6. — **A**, SEM-EDS analysis of the cement fraction in facies A of core St99. The EDS analysis indicated that the cement consists of low-magnesium calcite with clay minerals and terrigenous components; **B**, SEM-EDS analysis of a lithoclasts in facies B of core st99; **B-I**, **B-II**, **B-III**, high-magnesium calcite cement in the matrix of kaolinite and organic matter. Scale bars: A, 5 µm; B, 250 µm.

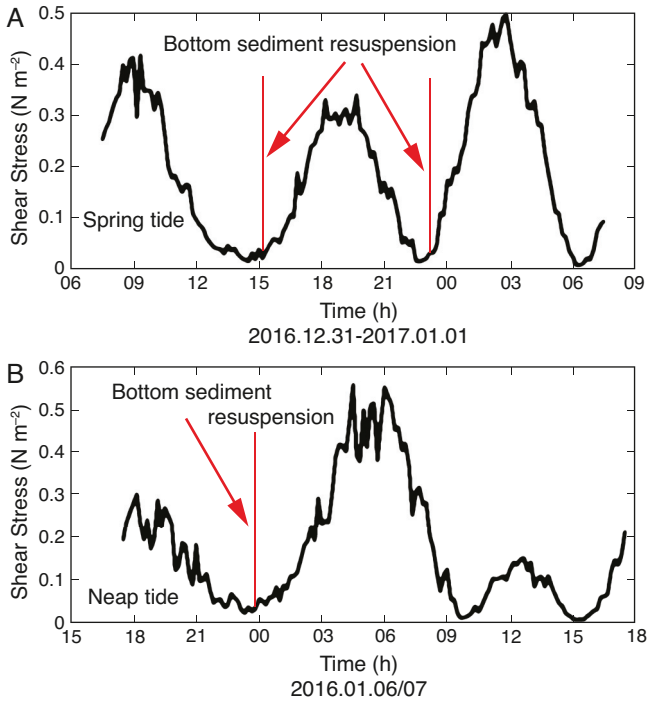

FIG. 7. — Nearbed shear stress estimated based on the Chahpahn station (rather northwest part of the PG) current data in: **A**, spring tide; **B**, neap tide.

Extremely warm climate of the PG region during the summer causes stagnant water in deep area of the PG that is associated with oxygen deficiency in the near bottom areas (Saleh *et al.* 2021) (Fig. S1.2). Oxygen deficiency reduces organic material decomposition that lead to OM increase in these areas. The hot weather condition is also prevalent during the Holocene that in turn has led to the formation of organic matter coated grains (Fig. 4).

Despite of high sediment supply by northern rivers and dust input as well as high bioproductivity, the sedimentation rate is not high in the PG except in river mouths and embayment areas (Hamzeh & Lahijani 2022). High renewal rate of the PG water (Vaezi & Lak 2023) (PGW) (Pous *et al.* 2015) and water circulation pattern could affect sediment distribution pattern. The finest sediment grain sizes are observed in the northern areas of the western and central basins of the Gulf where the bottom current reached to its minimum. Presence of the coarse grain sediments in some deep parts of the PG could be attributed to the impact of density driven currents that are theoretically be able to remove the finer portion of the sediments (Hamzeh 2021). However, Pous *et al.* (2015) demonstrated that the density driven currents in the PG are too weak to mobilize the bottom sediments; instead the density driven currents play a major role in flushing away the suspended and dissolved materials. Spatio-temporal changes in near bed turbulence significantly could change the threshold shear for sediment resuspension (Yang *et al.* 2019). Estimated near-bed shear stress based on current measurements in Chahpahn station in the PG demonstrate the threshold of bottom erosion (Fig. 7). More *in situ* measurements required for quantification of bottom sediment erosion and removal from the PG.

The mineralogical data suggested four important terrestrial sources of sediment in the PG: 1) Mesopotamia (aeolian); 2) Aghajari Formation of Zagros (alluvial); 3) Hormuz series (salt dome erosion); and 4) Tarus mountains (fluvial). Aeolian imports under the influence of the summer Shamal wind activities could be the most important extra-basin source of sediment. Mineralogical composition in the coastal area is more dependent on lithological and morphological properties. In the northern PG from the east to the west low-lying, low energy river-dominated coasts changed to steep slopes, high energy of rocky coasts (Baltzer & Purser 1990; Pourkerman *et al.* 2020). The energy of environment and erosion of bedrocks contributed to the mineralogical composition that is different in the northwest compared to the northeast PG. Geochemical and optical mineralogical analyses in high-energy deltaic systems reveal the presence of numerous reworked heavy minerals, such as chromite. These minerals are likely derived from the Oligo-Miocene sequences of the Zagros (Aghajari Formation). The Aghajari Formation, characterized by its thick clastic deposits, comprises fluvial sediments that have undergone significant weathering and erosion (Bahrami 2009; Pourkermana *et al.* 2017; Vaezi & Lak 2023).

The correlation matrix of marine surface and coastal sediments (Fig. 8A) reveals both positively and negatively correlated mineral groups. Some clay minerals, such as kaolinite and dickite, exhibit positive associations but display negative correlations with calcite. The weak association between calcite and aragonite may indicate two dominant sources: terrigenous for calcite and in biochemical source for aragonite. Minerals originating from crystalline rocks form three positively correlated groups, which include some carbonate minerals. These groups may represent the surrounding catchment areas and uplifted islands in the PG. Some uplifted islands expose the Precambrian series (Hormoz Complex), which are rich in salt as well as magmatic and metamorphic rocks. Their mineral signatures, such as tobermorite, are highlighted in the sediments around these islands.

The minerals have been categorized into four groups and utilized in ternary diagrams (Fig. 8B-E) for marine surface and coastal sediments, as well as two short cores. These diagrams indicate more diversified sources for the modern sediments, with dominant contributions from eolian and terrigenous sources, likely originating from the uplifted islands and the Zagros Mountains.

Finally, coastal sediment in the eastern part of the PG is associated by calcite, dolomite and anhydrite that generally resulted from salt domes erosion. Clay mineralogical studies for the PG demonstrated that palygorskite, smectite, illite, and chlorite are the main minerals for fractions smaller than 2 µm. Meanwhile, the abundance of kaolinite in the studied sediment, especially in the coastal area, could be the result of shale lithoclasts that were transported from the marl section of Aghajari Formation. Abundance of kaolinite in this part of the PG could be attributed to the transportation of shell fragments form marly sections of the Aghajari Formation, where we could see activities of salt domes in the coastal zone. The presence of chromite mineral on the shores of Dopalangan is another proof of sediment transfer from the Zagros (Aghajari Formation).

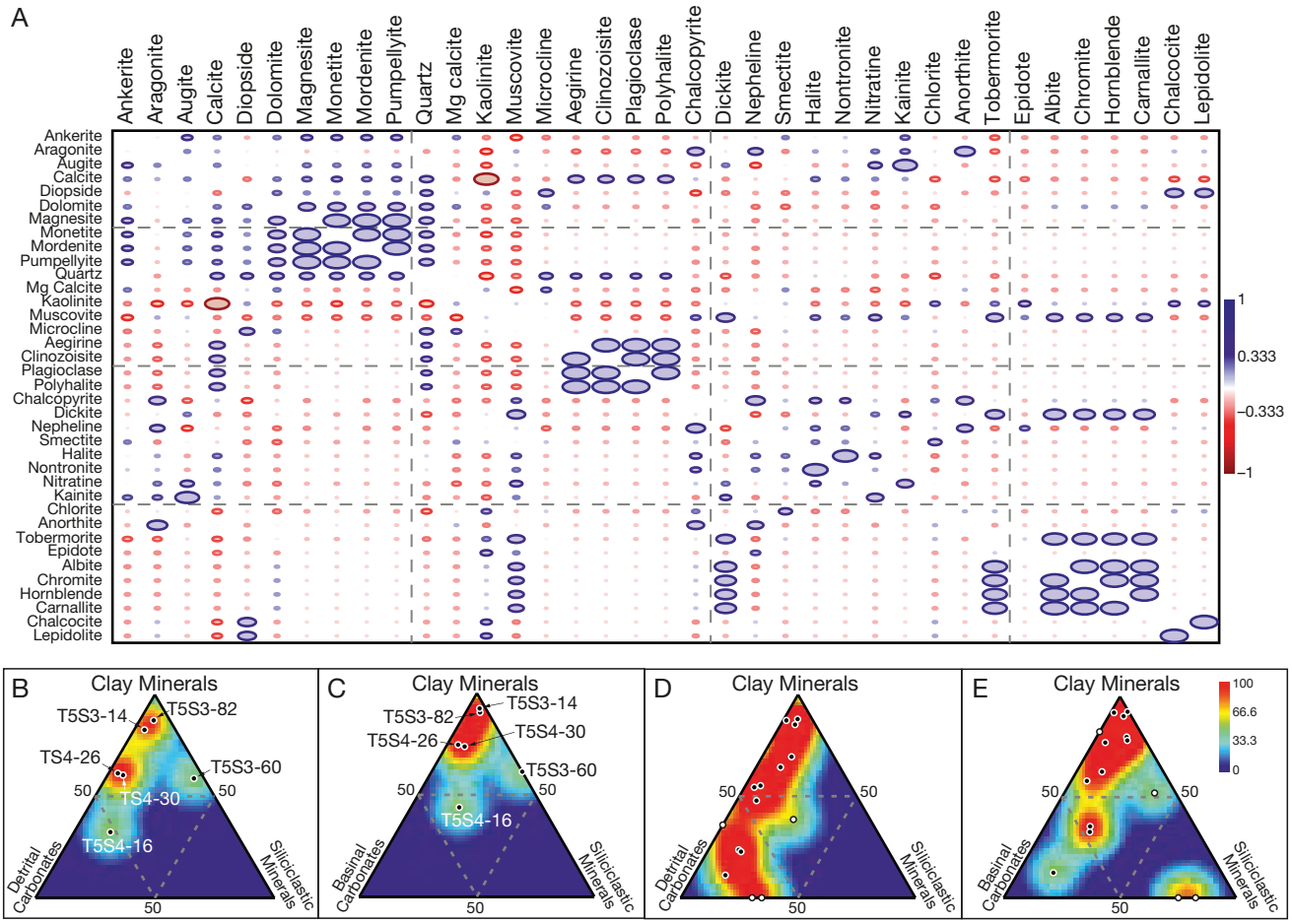

FIG. 8. — **A**, Correlation matrix of minerals for marine surface and coastal sediments; **B**, **C**, ternary diagrams for marine surface and coastal sediments; **D**, **E**, ternary diagrams for marine cores. Here minerals are groped in four following categories: 1) basinal carbonates (Aragonite, Monetite, Polyhalite, Chalcopyrite, Halite, Carnallite, Chalcocite, and Nitratine); 2) siliciclastic minerals (Plagioclase, Diopside, Mordenite, Pumpellyite, Quartz, Microcline, Aegirine, Clinozoisite, Nepheline, Kainite, Anorthite, Tobermorite, Epidote, Albite, Chromite, Hornblende, Lepidolite, Biotite, Amesite); 3) clay minerals (Kaolinite, Muscovite, Dickite, Smectite, Nontronite, Lepidolite); and 4) detrital carbonates (Ankerite, Calcite, Dolomite, Magnesite, Mg calcite).

Moving coarse sediments over marine bed by submarine currents is main reason to generation coating grains. Presence of dissolution traces over and inside ooids is attested by periodically environmental changes . During periods of stagnant water conditions, hypoxic or anoxic environments develop, leading to the precipitation of organic matter onto sediment grains. Conversely, when vertical mixing intensifies, the increased water movement enhances oxygen levels, resulting in the oxidation of the organic matter coating the sediment grains (Canfield 1993; Lau *et al.* 2024).

Sedimentary environment since Mid-Holocene

The Holocene sediments in the PG display role of basin morphology and governing climate, where in the southern parts are composed more carbonate and evaporite and in the north are mixed clastic and carbonate (Shinn 1973; Wagner & Van der Togt 1973; Baltzer & Purser 1990). Signature of the past climate events is reflected as changes in dust, clastic and biogenic and carbonate components. The Holocene sedimentation in the PG began when the sea level rose and flooded the low-land desert area that was crossed by rivers flowing to the Gulf of Oman (Kennett & Kennett 2007; Hosseinyar *et al.* 2021). From 7500 to 6500 cal yr BP, the central basin had a warm shallow marine environment with arid climate conditions (high dust storm events). During this time, marine cement with terrigenous silt was formed. Between 6500 and 5200 cal yr BP, the sea level in the PG rose rapidly and created an anoxic condition at the basin floor. This resulted in a decrease in benthos species and an increase in coated grains. This trend continued until 4200 cal yr BP, when the relative sea level reached its maximum.

The sea level in the central part of the PG reached its highest point in 6500 cal yr BP, but the evidence of highstand was found later, between 5290 and 4570 cal yr BP, in the southern PG (Lokier *et al.* 2015; Pourkerman *et al.* 2020). The sea level in the PG dropped around 4200 cal yr BP. The coastal cores show evidence of a sea level drop between 2500 and 1400 cal yr BP. The sea level in the PG was 3 meters lower than the current level at most during this period, according to Pourkerman *et al.* (2021). The sea level started to rise after 1400 cal yr BP and after a highstand in 1000 cal yr BP (Damien *et al.* 2020), the sea level in the PG at the current level.

CONCLUSION

The composition and particle size of the bottom sediments in the PG were investigated and found to be influenced by factors within the basin (such as environmental energy and water column stratification) and sediment supply from the catchment area (including rivers and islands). The major sources of terrigenous sediments are from Zagros and Taurus mountains. Olivine and moissanite minerals have been found in the surface sediments of the PG, which have not been seen in coastal sediments. This phenomenon shows that their origin is probably from the Tarus and Zagros ophiolites, which enter the PG through the Karun, Tigris and Euphrates rivers. Also, this phenomenon shows that the origin of coastal and sea bottom sediments has partially different sources.

The sediment grain size and mineralogical properties in the middle part of the PG are controlled by coastal energy and morphology. In this section, steep coasts and cliffs are dominant. The coarse-grained sediments of the deep bottom area of the PG have a high percentage of organic matter. Stagnant water condition due to warming caused oxygen deficiency in deep bottom areas that led to preservation of OM in the modern sediments and in the Middle Holocene. The sediment cores showed signs of reduction conditions that associated with buried OM around the sediment grains. The abundance of coated grains in the central basin could indicate a rapid rise of sea level in the PG.

Also, we found that some parts of the PG have low amount of clay sediment where high energy tidal current prevents calm environmental condition for sedimentation and rapid flushing transports fine materials into the Gulf of Oman.

The PG sediment composition displays strong imprint of dominant environmental conditions both in the PG itself and in the catchment basin. In the northern PG it shows mixed sedimentation of carbonate and clastic sediments. The current global warming and regional environmental changes could affect on the future sedimentation in the PG by reduction in fluvial supply, elevated dust sources and preservation of biogenic sediments.

Acknowledgements
This research has been supported by the Iran National Science Foundation (INSF) from the project "Sedimentary Atlas of the northern half of the Persian Gulf" number: 99001588, as well as research facilities from the Iranian National Institute for Oceanography and Atmospheric Science (INIOAS). Two anonymous referees are also thanked for their remarks on a previous version of the article.

REFERENCES

Al-Ansari E. M., Rowe G., Abdel-Moati M., Yigiterhan O., Al-Maslamani I., Al-Yafei M., Al-Shaikh I. & Upstill-Goddard R. 2015. — Hypoxia in the central Arabian Gulf Exclusive Economic Zone (EEZ) of Qatar during summer season. *Estuarine, Coastal and Shelf Science* 159: 60-68. https://doi.org/10.1016/j.ecss.2015.03.022

Al-Dousari A., Doronzo D. & Ahmed M. 2017. — Types, indications and impact evaluation of sand and dust storms trajectories in the Arabian Gulf. *Sustainability* 9 (9): 114. https://doi.org/doi.org/10.3390/su9091526

Al-Ghadban A., Abdali F. & Massoud M. 1998. — Sedimentation rate and bioturbation in the Arabian Gulf. *Environment International* 24 (1-2): 23-31. https://doi.org/10.1016/S0160-4120(97)00118-9

Awadh S., Ali M. & Ali R. 2011. — Mineralogy and palynology of the Mesopotamian plain sediments, Central Iraq. *Arabian Journal of Geosciences* 4: https://doi.org/10.1007/s12517-010-0161-y

Azizpour J., Siadatmousavi S. M. & Chegini V. 2016. — Measurement of tidal and residual currents in the Strait of Hormuz. *Estuarine, Coastal and Shelf Science* 178: 101-109. https://doi.org/10.1016/j.ecss.2016.06.004

Azizpour J., Chegini V., Khosravi M. & Einali A. 2014. — Study of the physical oceanographic properties of the persian gulf, strait of hormuz and gulf of oman based on PG-GOOS CTD measurements. *Journal of Persian Gulf* 5 (18): 37-48. https://iranjournals.nlai.ir/handle/123456789/542938

Bahrami M. 2009. — Lithofacies and sedimentary environments of Aghajari Formation in Dehsheikh Mountain, west of Shiraz, Iran. *World Applied Sciences Journal* 6 (4): 464-473.

Baltzer F. & Purser B. H. 1990. — Modern alluvial fan and deltaic sedimentation in a foreland tectonic setting: the lower Mesopotamian plain and the Arabian Gulf. *Sedimentary Geology* 67 (3-4): 175-197. https://doi.org/10.1016/0037-0738(90)90034-Q

Beni A. N., Marriner N., Sharifi A., Azizpour J., Kabiri K., Djamali M. & Kirman A. 2021. — Climate change: A driver of future conflicts in the Persian Gulf Region? *Heliyon* 7 (2): e06288. https://doi.org/10.1016/j.heliyon.2021.e06288

Berry R. W., Brophy G. P. & Naqash A. 1970. — Mineralogy of the suspended sediment in the Tigris, Euphrates, and Shatt-al-Arab rivers of Iraq, and the recent history of the Mesopotamian Plain. *Journal of Sedimentary Research* 40 (1): 131-139. https://doi.org/10.1306/74D71F05-2B21-11D7-8648000102C1865D

Canfield D. E. 1993. — Organic matter oxidation in marine sediments, *in* Conference proccedings, *Interactions of C, N, P and S Biogeochemical Cycles and Global Change*. Springer Heidelberg: 333-363. https://doi.org/10.1007/978-3-642-76064-8_14

Chao S. Y., Kao T. W. & Al Hajri K. R. 1992. — A numerical investigation of circulation in the Arabian Gulf. *Journal of Geophysical Research: Oceans* 97 (C7): 11219-11236. https://doi.org/10.1029/92JC00841

Damien A., Kosmas P. & Éric F. 2020. — Holocene relative sea-level variations and archeological implications, Abu Dhabi western region, United Arab Emirates. *Arabian Journal of Geosciences* 13: 1-16. https://doi.org/10.1007/s12517-020-5155-9

Dauner A. L. L., Mollenhauer G., Hefter J., Bicego M. C., de Mahiques M. M. & Martins C. d. C. 2022. — Late Pleistocene to Holocene variations in marine productivity and terrestrial material delivery to the western South Atlantic. *Frontiers in Marine Science* 9: 924556. https://doi.org/10.3389/fmars.2022.924556

Einsele G. 1996. — Event deposits: the role of sediment supply and relative sea-level changes – overview. *Sedimentary Geology* 104 (1-4): 11-37. https://doi.org/10.1016/0037-0738(95)00118-2

Evans G., Schmidt V., Bush P. & Nelson H. 1969. — Stratigraphy and geologic history of the sabkha, Abu Dhabi, Persian Gulf. *Sedimentology* 12 (1-2): 145-159. https://doi.org/10.1111/j.1365-3091.1969.tb00167.x

Folk L. 1980. — *Petrology of Sedimentary Rocks*. Hamphill, Austin, Texas, 184 p. http://hdl.handle.net/2152/22930

Garzanti E., Al-Juboury A. I., Zoleikhaei Y., Vermeesch P., Jotheri J., Akkoca D. B., Obaid A. K., Allen M. B., Andó S. & Limonta M. 2016. — The Euphrates-Tigris-Karun river system: Provenance, recycling and dispersal of quartz-poor foreland-basin sediments in arid climate. *Earth-Science Reviews* 162: 107-128. https://doi.org/10.1016/j.earscirev.2016.09.009

GHAFARIAN P., KABIRI K., DELJU A. H. & FALLAHI M. 2022. — Spatio-temporal variability of dust events in the northern Persian Gulf from 1991 to 2020. *Atmospheric Pollution Research* 13 (4): 101357. https://doi.org/10.1016/j.apr.2022.101357

GHAZBAN F. 2009. — *Petroleum Geology of the Persian Gulf*. Tehran University Press, 707 p.

GISCHLER E. & LOMANDO A. J. 2005. — Offshore sedimentary facies of a modern carbonate ramp, Kuwait, northwestern Arabian-Persian Gulf. *Facies* 50: 443-462. https://doi.org/10.1007/s10347-004-0027-4

HAMZEH M. & LAHIJANI H. 2022. — Soil and Vegetative Carbon Sequestration in Khuran Estuary Mangroves, Strait of Hormoz, During the Last 18 Centuries. *Estuaries and Coasts* 45 (6): 1583-1595. https://doi.org/10.1007/s12237-021-01037-7

HAMZEH M. A. 2021. — Environmental implications of the distribution and physical characteristics of surface sediments in the northern Persian Gulf. *Geo-Marine Letters* 41 (4): 1-15. https://doi.org/10.1007/s00367-021-00716-5

HAMZEH M. A., KHOSRAVI M., CARTON X., YARAHMADI D. & SAFARKHANI E. 2021. — Paleoceanography of the Strait of Hormoz and its link to paleoclimate changes since the mid-Holocene. *Continental Shelf Research* 226: 104507. https://doi.org/10.1016/j.csr.2021.104507

HASSAN A. 2018. — The environmental geomorphological assessment of the urban expansion in Al-Khiran Marine City, Kuwait. *Journal of the Society of the Scientific Kuwait University* 46 (1): 31-54. https://doi.org/10.34120/0080-046-001-010

HOSSEINYAR G., BEHBAHANI R., MOUSSAVI-HARAMI R., LAK R. & KUIJPERS A. 2021. — Holocene sea-level changes of the Persian Gulf. *Quaternary International* 571: 26-45. https://doi.org/10.1016/j.quaint.2020.11.051

HOUBOLT J. 1957. — *Surface Sediments of the Persian Gulf near the Qatar Peninsula*. Vol. 113. Mouton and Co, The Hague, 186 p.

JIN Z., YU J., ZHANG F. & QIANG X. 2020. — Glacial-interglacial variation in catchment weathering and erosion paces the Indian summer monsoon during the Pleistocene. *Quaternary Science Reviews* 248: 106619. https://doi.org/10.1016/j.quascirev.2020.106619

JOHNS W., YAO F., OLSON D., JOSEY S., GRIST J. & SMEED D. 2003. — Observations of seasonal exchange through the Straits of Hormuz and the inferred heat and freshwater budgets of the Persian Gulf. *Journal of Geophysical Research: Oceans* 108 (C12): https://doi.org/10.1029/2003JC001881

KÄMPF J. & SADRINASAB M. 2006. — The circulation of the Persian Gulf: a numerical study. *Ocean Science* 2 (1): 27-41. https://doi.org/10.5194/os-2-27-2006, 2006

KAMRANZAD B., ETEMAD-SHAHIDI A. & CHEGINI V. 2013. — Assessment of wave energy variation in the Persian Gulf. *Ocean Engineering* 70: 72-80. https://doi.org/10.1016/j.oceaneng.2013.05.027

KARS M., MUSGRAVE R. J., KODAMA K., JONAS A.-S., BORDIGA M., RUEBSAM W., MLENECK-VAUTRAVERS M. J. & BAUERSACHS T. 2017. — Impact of climate change on the magnetic mineral assemblage in marine sediments from Izu rear arc, NW Pacific Ocean, over the last 1 Myr. *Palaeogeography, Palaeoclimatology, Palaeoecology* 480: 53-69. https://doi.org/10.1016/j.palaeo.2017.05.016

KENDALL C. G. S. C. & SKIPWITH P. A. D. E. 1969. — Holocene shallow-water carbonate and evaporite sediments of Khor al Bazam, Abu Dhabi, southwest Persian Gulf. *AAPG Bulletin* 53 (4): 841-869. https://doi.org/10.1306/5D25C803-16C1-11D7-8645000102C1865D

KENNETT D. J. & KENNETT J. P. 2007. — Influence of Holocene marine transgression and climate change on cultural evolution in southern Mesopotamia, *Climate Change and Cultural Dynamics*. Elsevier: 229-264. https://doi.org/10.1016/B978-012088390-5.50012-1

KONYUHOV A. & MALEKI B. 2006. — The Persian Gulf Basin: Geological history, sedimentary formations, and petroleum potential. *Lithology and Mineral Resources* 41 (4): 344-361. https://doi.org/10.1134/S0024490206040055

KUKAL Z. & SAADALLAH A. 1973. — Aeolian admixtures in the sediments of the northern Persian Gulf, *in* PURSER B. H. (ed.), *The Persian Gulf – Holocene Carbonate Sedimentation and Diagenesis in a Shallow Epicontinental Sea*. Springer, Berlin, Heidelberg: 115-121. https://doi.org/10.1007/978-3-642-65545-6_7

LACHKAR Z., MEHARI M., LEVY M., PAPARELLA F. & BURT J. A. 2022. — Recent expansion and intensification of hypoxia in the Arabian Gulf and its drivers. *Frontiers in Marine Science* 9: 891378. https://doi.org/10.3389/fmars.2022.891378

LAMBECK K. 1996. — Shoreline reconstructions for the Persian Gulf since the last glacial maximum. *Earth and Planetary Science Letters* 142 (1-2): 43-57. https://doi.org/10.1016/0012-821X(96)00069-6

LAU M. P., HUTCHINS R. H., TANK S. E. A. & DEL GIORGIO P. 2024. — The chemical succession in anoxic lake waters as source of molecular diversity of organic matter. *Scientific Reports* 14 (1): 3831. https://doi.org/10.1038/s41598-024-54387-0

LI M. Z., HANNAH C. G., PERRIE W. A., TANG C. C., PRESCOTT R. H. & GREENBERG D. A. 2015. — Modelling seabed shear stress, sediment mobility, and sediment transport in the Bay of Fundy. *Canadian Journal of Earth Sciences* 52 (9): 757-775. https://doi.org/10.1139/cjes-2014-0211

LOKIER S. W., BATEMAN M. D., LARKIN N. R., RYE P. & STEWART J. R. 2015. — Late Quaternary sea-level changes of the Persian Gulf. *Quaternary Research* 84 (1): 69-81. https://doi.org/10.1016/j.yqres.2015.04.007

MAHIQUES M. M. DE, TESSLER M. G., CIOTTI A. M., DA SILVEIRA I. C. A., SOUSA S. H. DE M. E, FIGUEIRA R. C. L., TASSINARI C. C. G., FURTADO V. V. & PASSOS R. F. 2004. — Hydrodynamically driven patterns of recent sedimentation in the shelf and upper slope off Southeast Brazil. *Continental Shelf Research* 24 (15): 1685-1697. https://doi.org/10.1016/j.csr.2004.05.013

MAHOWALD N., KOHFELD K., HANSSON M., BALKANSKI Y., HARRISON S. P., PRENTICE I. C., SCHULZ M. & RODHE H. 1999. — Dust sources and deposition during the last glacial maximum and current climate: A comparison of model results with paleodata from ice cores and marine sediments. *Journal of Geophysical Research: Atmospheres* 104 (D13): 15895-15916. https://doi.org/10.1029/1999JD900084

MOGHADAM H. S. & STERN R. J. 2011. — Geodynamic evolution of Upper Cretaceous Zagros ophiolites: formation of oceanic lithosphere above a nascent subduction zone. *Geological Magazine* 148 (5-6): 762-801. https://doi.org/10.1017/S0016756811000410

NADERI BENI A., LEDUC G., DJAMALI M., SHARIFI A., MARRINER N., TACHIKAWA K., ROSTEK F., TJALLINGII R., LAHIJANI H., MOLAVI ARABSHAHI M., GARCIA M., LICARI L., TETARD M., BELLINGHERY M.-C., BARD E. 2024. — Postglacial flooding and Holocene climate shifts in the Persian Gulf. *Journal of Quaternary Science* 39 (4): 592-607. https://doi.org/10.1002/jqs.3614

NAJAFPOUR N., EMAMGHOLIZADEH S., TORABI POUDEH H. & HAGHIABI A. H. 2016. — Estimation of Sediment Transport Rate of Karun River (Iran). *Journal of Hydraulic Structures* 2 (2): 74-84. https://doi.org/10.22055/jhs.2016.12874

NOAA 2024. — National Oceanic and Atmospheric Administration (NOAA) Coral Reef Watch. NOAA, United States.

ORANG K., MOTAMEDI H., AZADIKHAH A. & ROYATVAND M. 2018. — Structural framework and tectono-stratigraphic evolution of the eastern Persian Gulf, offshore Iran. *Marine and Petroleum Geology* 91: 89-107. https://doi.org/10.1016/j.marpetgeo.2017.12.014

PHILIP G. 1968. — Mineralogy of the Recent sediments of Tigris and Euphrates rivers and some of the older detrital deposits. *Journal of Sedimentary Research* 38 (1): 35-44. https://doi.org/10.1306/74D718C0-2B21-11D7-8648000102C1865D

POURKERMAN M., MARRINER N., MORHANGE C., DJAMALI M., SPADA G., AMJADI S., VACCHI M., LAHIJANI H., JELODAR M. E. & TOFIGHIAN H. 2020. — Geoarchaeology as a tool to understand ancient navigation in the northern Persian Gulf and the harbour history of Siraf. *Journal of Archaeological Science: Reports* 33: 102539. https://doi.org/10.1016/j.jasrep.2020.102539

Pourkerman M., Marriner N., Morhange C., Djamali M., Lahijani H., Amjadi S., Vacchi M., Jelodar M. E., Spada G. & Tofighian H. 2021. — Late Holocene relative sea-level fluctuations and crustal mobility at Bataneh (Najirum) archaeological site, Persian Gulf, Iran. *Geoarchaeology* 36 (5): 740-754. https://doi.org/10.1002/gea.21860

Pourkermana M., Amjadi S., Naderi Beni A., Lahijani H. & Mehdinia A. 2017. — Evaluation of metal contamination in the Mand River delta, Persian Gulf. *Marine Pollution Bulletin*: https://doi.org/10.1016/j.marpolbul.2017.05.003

Pous S., Carton X. J. & Lazure P. 2013. — A process study of the wind-induced circulation in the Persian Gulf. *Open Journal of Marine Science* 3 (1): 27160. https://doi.org/10.4236/ojms.2013.31001

Pous S., Lazure P. & Carton X. 2015. — A model of the general circulation in the Persian Gulf and in the Strait of Hormuz: Intraseasonal to interannual variability. *Continental Shelf Research* 94: 55-70. https://doi.org/10.1016/j.csr.2014.12.008

Purser B. 1973. — Sedimentation around bathymetric highs in the southern Persian Gulf, *The Persian Gulf*. Springer: 157-177.

Purser B. & Seibold E. 1973. — The principal environmental factors influencing Holocene sedimentation and diagenesis in the Persian Gulf, *in* Purser B. H. (ed.), *The Persian Gulf – Holocene Carbonate Sedimentation and Diagenesis in a Shallow Epicontinental Sea*. Springer, Berlin, Heidelberg. Springer: 1-9. https://doi.org/10.1007/978-3-642-65545-6_1

Reynolds R. M. 1993. — Physical oceanography of the Gulf, Strait of Hormuz, and the Gulf of Oman – Results from the Mt Mitchell expedition. *Marine Pollution Bulletin* 27: 35-59. https://doi.org/10.1016/0025-326X(93)90007-7

Sahraeyan M. 2013. — Sedimentology and palaeogeography of conglomerates from the Aghajari Formation in Zagros Basin, SW Iran. *International Journal of Advanced Geosciences* 1: 13-22. https://doi.org/10.14419/ijag.v1i1.842

Saleh A., Abtahi B., Mirzaei N., Chen C.-T. A., Ershadifar H., Ghaemi M., Hamzehpour A. & Abedi E. 2021. — Hypoxia in the Persian Gulf and the Strait of Hormuz. *Marine Pollution Bulletin* 167: 112354. https://doi.org/10.1016/j.marpolbul.2021.112354

Saleh D. K. 2010. — *Stream Gage Descriptions and Streamflow Statistics for Sites in the Tigris River and Euphrates River Basins, Iraq*. USGS.

Schumacher B. A. 2002. — Methods for the determination of total organic carbon (TOC) in soils and sediments. *Ecological Risk Assessment Support Center* 2002: 1-23.

Seibold E. & Vollbrecht K. 1969. — Die Bodengestalt des Persischen Golfs, *in* Seibold E. & Closs H. (eds), *Meteor Forschungsergebnisse: Herausgegeben von der Deutschen Forschungsgesellschaft*. Gebruder Borntraeger, Berlin: 31-56.

Seibold E., Diester L., Fütterer D., Lange H., Müller P. & Werner F. 1973. — Holocene sediments and sedimentary processes in the Iranian part of the Persian Gulf, *in* Purser B. H. (ed.), *The Persian Gulf – Holocene Carbonate Sedimentation and Diagenesis in a Shallow Epicontinental Sea*. Springer, Berlin, Heidelberg. Springer: 57-80. https://doi.org/10.1007/978-3-642-65545-6_4

Shinn E. 1973. — Recent intertidal and nearshore carbonate sedimentation around rock highs, E Qatar, Persian Gulf, *in* Purser B. H. (ed.), *The Persian Gulf – Holocene Carbonate Sedimentation and Diagenesis in a Shallow Epicontinental Sea*. Springer, Berlin, Heidelberg. Springer: 193-198. https://doi.org/10.1007/978-3-642-65545-6_11

Sugden W. 1963. — The hydrology of the Persian Gulf and its significance in respect to evaporite deposition. *American Journal of Science* 261 (8): 741-755. https://doi.org/10.2475/ajs.261.8.741

Swift S. A. & Bower A. S. 2003. — Formation and circulation of dense water in the Persian/Arabian Gulf. *Journal of Geophysical Research: Oceans* 108 (C1): 4-1-4-21. https://doi.org/10.1029/2002JC001360

Uchupi E., Swift S. A. & Ross D. A. 1996. — Gas venting and late Quaternary sedimentation in the Persian (Arabian) Gulf. *Marine Geology* 129 (3-4): 237-269. https://doi.org/10.1016/0025-3227(96)83347-0

Uchupi E., Swift S. A. & Ross D. A. 1999. — Late Quaternary stratigraphy, paleoclimate and neotectonism of the Persian (Arabian) Gulf region. *Marine Geology* 160 (1): 1-23. https://doi.org/10.1016/S0025-3227(99)00011-0

UN-ESCWA & BGR 2013. — Inventory of Shared Water Resources in Western Asia: United Nations Economic and Social Commission for Western Asia and Bundesanstalt für Geowissenschaften und Rohstoffe. https://www.unescwa.org/

Vaezi A. & Lak R. 2023. — Sediment Texture, Geochemical Variation, and Ecological Risk Assessment of Major Elements and Trace Metals in the Sediments of the Northeast Persian Gulf. *Minerals* 13 (7): 850. https://doi.org/10.3390/min13070850

Wagner C. & Van der Togt C. 1973. — Holocene sediment types and their distribution in the southern Persian Gulf, *in* Purser B. H. (ed.), *The Persian Gulf – Holocene Carbonate Sedimentation and Diagenesis in a Shallow Epicontinental Sea*. Springer, Berlin, Heidelberg. Springer: 123-155. https://doi.org/10.1007/978-3-642-65545-6_8

Warren J. K. 2010. — Evaporites through time: Tectonic, climatic and eustatic controls in marine and nonmarine deposits. *Earth-Science Reviews* 98 (3-4): 217-268. https://doi.org/10.1016/j.earscirev.2009.11.004

Yang Y., Gao S., Wang Y. P., Jia J., Xiong J. & Zhou L. 2019. — Revisiting the problem of sediment motion threshold. *Continental Shelf Research* 187: 103960. https://doi.org/10.1016/j.csr.2019.103960

Zittis G., Almazroui M., Alpert P., Ciais P., Cramer W., Dahdal Y., Fnais M., Francis D., Hadjinicolaou P. & Howari F. 2022. — Climate change and weather extremes in the Eastern Mediterranean and Middle East. *Reviews of Geophysics* 60 (3): e2021RG000762. https://doi.org/10.1029/2021RG000762

Submitted on 7 February 2024;
accepted on 16 September 2024;
published on 23 September 2025.

Appendix 1. — Supplementary Figures associated to the article: https://doi.org/10.5852/geodiversitas2025v47a14_s1